J. Fluid Mech. (2006), *vol.* 552, *pp.* 37–71.
doi:10.1017/S0022112005008475 Printed in the United Kingdom

Thin-film flow of a viscoelastic fluid on an axisymmetric substrate of arbitrary shape

By ROGER E. KHAYAT[1] AND KYU-TAE KIM[2]

[1]Department of Mechanical and Materials Engineering, The University of Western Ontario, London, Ontario, Canada N6A 5B9
rkhayat@uwo.ca

[2]Industrial Materials Institute, National Research Council of Canada, Boucherville, Quebec, Canada

(Received 7 April 2005 and in revised form 12 September 2005)

The interplay between inertia and elasticity is examined in this study for the transient axisymmetric flow of a thin film. The fluid is assumed to emerge from an annulus, as it is driven by axial pressure gradient and/or gravity. The substrate is assumed to be stationary and of arbitrary shape. The boundary-layer equations are generalized for a viscoelastic film obeying the Oldroyd-B constitutive model. These equations are solved by expanding the flow field in terms of orthonormal shape functions in the radial direction and using the Galerkin projection, combined with a time-stepping implicit scheme, and integration along the flow direction. It is found that the viscosity ratio and fluid elasticity can have a significant effect on steady state as well as transient behaviour. It is also found that low-inertia and/or highly elastic fluids tend to accumulate near the annulus, exhibiting a standing wave that grows with time. This behaviour clearly illustrates the difficulty associated with coating viscoelastic high-viscosity fluids. A criterion for film rupture is also established, which is based on the steepening of flow and stress gradients. The topography of the substrate has a drastic effect on the flow as well.

1. Introduction

This study examines the role of elasticity during the early stages of development of a viscoelastic film emerging from an annulus and moving on a solid substrate of axisymmetric shape. Steady flow and its stability are also examined. Other influencing factors and their interplay with elasticity, such as inertia, gravity and substrate topography, are also investigated. The study is obviously of close relevance to coating flow (Weinstein & Ruschak 2004). Although steady film flow on a substrate has been extensively investigated, little work has been devoted to transient behaviour. This is of course understandable since it is the long-term behaviour, after transient effects have subsided, that is usually of practical interest. However, when difficulties are encountered in film flow processing, the origin of these difficulties may lie in the initial stages of the process, long before the flow reaches steady state. More importantly, the steady state may not be stable under some processing conditions, particularly for polymeric films. It is thus crucial to examine initial transients, which may allow early control of potential problems in practice. The time it takes a film process to reach steady state is by itself an important issue. Polymeric fluids exhibit different relaxation times, and therefore, different transient responses. The film flow can also be inherently transient as a result of geometrical variations or continuous changes in processing conditions.

Understandably, thin-film flow has mostly been examined for Newtonian fluids (Brourgin 1997; Kistler & Schweizer 1997). To a much lesser extent, non-Newtonian film flows have also been considered (Szeri 1987; Larson 1992). Generally, most studies involve either gravity- and/or surface-tension-driven flow (Quéré 1990; Chang 1994; Oron, Davis & Bankoff 1997; Meyers 1998). The effect of substrate topography was considered by Kalliadasis, Bielarz & Homsy (2000) on the steady thin-film flow over trenches and mounds. Mazouchi & Homsy (2001) compared the solution to two-dimensional Stokes flow to their earlier thin-film based solution. This comparison indicated that the thin-film hypothesis remains valid even in the presence of steep topographic variation. Mazouchi & Homsy (2001) attributed this validity to the smoothing role that surface tension effects tend to play. Their study was limited, however, to surface-tension dominated inertialess flow. Ruschak & Weinstein (1999) examined gravity-driven flow of a thin film over a round-crested weir. Similarly to the present problem, the surface tension effect was neglected, and the inertia effect was included.

Transient flow studies are often limited to the linear destabilization of the film or to small-amplitude motion (Frenkel 1992; Larson 1992; Chang 1994). Studies on finite-amplitude film deformation include the radial spreading in spin coating (Watson 1964), the evaporation of liquid films (Burelbach, Bankoff & Davis 1988), the instability and breakup of long annular liquid layers (Mashayek & Ashgriz 1995; de Bruyn 1997), and the evolution of a falling film (Pumir, Manneville & Pomeau 1983; Takeshi 1999). Of closer relevance to the present problem, is the simulation of Kalliadasis & Chang (1994), who examined the critical conditions for the formation of solitary waves during the coating of vertical fibres. The long-wave equation was solved using a matched asymptotic expansion, which joins the capillary outer region of the large solitary wave to the thin-film inner region. Inertia was neglected. Nguyen & Balakotaiah (2000) proposed an integral boundary-layer model for a free-falling film.

The present study incorporates nonlinearities stemming from both inertia and elasticity. The interplay between inertia and other forces in thin-film flow has been examined in the literature. Szeri (1987) reviewed some of the attempts made to extend the classical Reynolds equation to include the effect of inertia in lubrication theory. In a review article on fibre coating, Quéré (1999) discussed the effect of inertia on rapid coating and droplet expulsion. For a general discussion on the role of inertia in free-surface flow, see Leal (1992). Of closer relevance to the present study is the work by Watson (1964), who examined the steady laminar and turbulent radial spread of a liquid jet over a horizontal plane, including the special case of two-dimensional flow. At large distance from the source, a similarity solution of the laminar boundary-layer equations was sought. In particular, Watson found that for two-dimensional flow, the steady (dimensionless) shape of the free surface is given by $\eta_s = \pi x/\sqrt{3}Re = 1.81x/Re$, where x is the distance from the source, and Re is the (modified) Reynolds number. The steady surface profile was obtained in the absence of gravity and surface tension. It constitutes an important limit form, which will be compared against the present formulation. Khayat & Welke (2001) examined the two-dimensional transient film flow. Comparison with Watson's similarity solution in this case led to good agreement.

Although the thin-film formulation reduces the pressure to its hydrostatic part, thus eliminating the momentum equation in the transverse (vertical or radial) direction from the problem, the dimension of the problem remains the same as in the original equation. Benney's (1966) long-wave (LW) approximation is often used, especially for small-inertia flow. At high Reynolds number, inertia is better accounted for through the 'boundary-layer' (BL) approximation, which includes the effect of transverse flow.

Salamon, Armstrong & Brown (1994) carried out a finite-element solution of the full Navier–Stokes equations for the flow in a falling film. Comparison of their results with those based on the LW approximation, indicates that serious limitations exist in the validity of the LW equation. The major difference between the original Navier–Stokes equations and the BL equations is the hydrostatic variation of the pressure across the film depth. As a result, only the transverse momentum equation is eliminated, but the convective terms are retained in the remaining equations, and the number of boundary conditions is reduced. However, the solution of the BL equations remains essentially as difficult to obtain as that of the Navier–Stokes equations (Takeshi 1999). A depthwise integration of the momentum equation(s) in the lateral direction(s) is usually performed by assuming a self-similar semi-parabolic flow profile in the transverse direction, as was proposed (Shkadov 1967). Although the depth-averaged equations are only of second order in time, they yield plausible results, at least qualitatively, but they remain fundamentally questionable because of the semi-parabolic assumption (Frenkel 1992; Takeshi 1999). A measure of the error involved may be inferred by computing the free-surface profile in the absence of gravity and surface tension, and comparing it to Watson's result given above. From the literature, the steady-state profile based on the semi-parabolic profile is easily found to be $\eta_s = 2.5x/Re$ (Chang 1994). The parabolic approximation is widely used in the literature, and its validity was established experimentally by Alekseenko, Nakoryakov & Pokusaev (1985). However, it is generally argued that the parabolic approximation is valid at low or moderately-low Reynolds number, and provided the waves are far from the entry (Wilkes & Nedderman 1962; Bertshy & Chin 1993). In addition to high-inertia flow, other flow conditions that restrict the range of validity of the semi-parabolic profile include the presence of end effects, turbulent flow, and (most likely) nonlinear effects stemming from shear-thinning or viscoelastic effects. A more rigorous approach for the solution of the thin-film equations becomes almost as difficult to achieve as for the original Navier–Stokes equations. Hence, conventional solution techniques such as the finite-element or finite-difference methods are not suitable, given the rapid spatio-temporal variation of the flow field in the presence of steep waves. Frequent re-meshing, and an effective implicit time-stepping scheme are required. Ruyer-Quil & Manneville (1998) used a three-term expansion of the flow field in the transverse direction, and obtained three coupled equations for the surface height, flow rate and stress. Takeshi examined the flow in a falling film at moderate Reynolds number and large but finite Weber number, using a regularization method, which consists of a combination of the Padé approximation and the long-wave expansion (Takeshi 1999).

The free-surface flow of non-Newtonian fluids remains relatively unexplored, particularly the flow of thin films. Spaid & Homsy (1994) examined the spin coating of Oldroyd-B fluid films. Fomin, Hashida & Watterson (2003) examined rimming flow on the inner surface of a horizontal rotating cylinder. Ro & Homsy (1995) examined the influence of elasticity on the meniscus shape and film thickness for the creeping flow induced by air injection into a Hele-Shaw cell, with significant surface tension. Gravity-driven non-Newtonian films have been examined by Kang & Chen (1995), also for creeping flow in the presence of surface-tension effects. Pasquali & Scriven (2002) examined the creeping flow around a cylinder in a channel, and the flow under the downstream section of a slot or knife coater. Lee, Shaqfeh & Khomani (2002) applied the finite-element methods to studying viscoelastic Hele-Shaw and slot coating flows. Bhatara, Shaqfeh & Khomani (2004) examined the interplay between gravity and surface-tension effects for the creeping flow induced by air displacing

a fluid. Surfactant-driven thin viscoelastic films have also been considered (Zhang, Matar & Craster 2002).

The evolution of thin-film flow typically involves three distinct stages, which are usually identified after flow inception (Khayat & Welke 2001). The first stage is the formation of a wave near the channel or annulus exit, the second stage is the propagation of the wave on the open substrate, and the third stage is the development of the steady-state flow. The present modelling and simulation of the three stages are performed for axisymmetric flow in order to examine the intricate wave and flow structures that develop for a viscoelastic film. The problem thus consists of obtaining the shape of the evolving free surface and the flow field inside the moving domain, as the fluid emerges from the annulus. The flow is pressure and/or gravity induced. In this study, a unified spectral approach is proposed to model the axisymmetric flow of a thin film over a substrate of arbitrary shape. Given the importance of inertia and normal stress upon inception, the BL formulation rather than Benney's LW approximation will be used. The flow equations are first mapped over the rectangular domain, and a formal spectral expansion of the velocity field in terms of orthonormal basis functions is introduced for the flow field.

Unlike the depth-averaging method, the spectral methodology used in the current study becomes particularly suited for the early onset of wave motion near the annulus exit. Assessment of convergence and accuracy is carried out by adopting different truncation levels, varying the time increment and mesh size, and monitoring the conservation of mass (volume). The overall validity of the basic approach is established by comparing the two-dimensional steady-state solution against the similarity solution of Watson (1964), and the solution based on the parabolic profile and the depth-averaging procedure (Chang 1994). More extensive validation of the proposed spectral methodology was carried out previously for the thin-film flow of Newtonian (Khayat & Welke 2001) and generalized Newtonian (Kim & Khayat 2002) fluids. The problem thus consists of obtaining the shape of the evolving free surface and the flow velocity inside a moving domain, as the fluid emerges from the annulus. Details of the free surface and flow field can be captured both explicitly and in the mean sense. The present study is focused on the interplay between inertia and elasticity, which are assumed to be the dominant effects in the flow. Conditions of shock formation, which lead unavoidably to film rupture, are particularly emphasized. Although some discussion and prediction of film rupture are included, surface-tension effects are assumed to be negligible. Film rupture is attributed to strong velocity gradient and, consequently, strong normal stress effect, rather than to film thinning as in Newtonian fluids. Finally, the effect of substrate topography will be examined in detail.

2. Problem formulation and solution procedure

In this section, the film flow configuration is introduced, and the scaled conservation and constitutive equations for a viscoelastic fluid film, as well as the boundary and initial conditions are briefly discussed. The solution procedure is then discussed in some detail.

2.1. *Governing equations, boundary and initial conditions*

The fluid is assumed to be an incompressible polymeric solution of density ρ, relaxation time λ, viscosity μ, and surface tension coefficient σ. In this study, only fluids that can be reasonably represented by a single relaxation time and constant viscosity are considered. The polymeric solution is assumed to be composed of a Newtonian

solvent of viscosity μ_s, and a polymeric solute of viscosity μ_p, such that the solution viscosity is given by $\mu = \mu_s + \mu_p$. Regardless of the nature of the fluid, the continuity and momentum balance equations must hold. The conservation equations for an incompressible fluid can be concisely written as:

$$\nabla \cdot \boldsymbol{U} = 0, \quad \rho(\boldsymbol{U}_{,T} + \boldsymbol{U} \cdot \nabla \boldsymbol{U}) = \nabla \cdot \boldsymbol{\Sigma} + \rho \boldsymbol{g}, \tag{2.1}$$

where $\boldsymbol{U}$ is the velocity vector, $\boldsymbol{g}$ is the acceleration due to gravity, T is the time, and ∇ is the gradient operator. A comma followed by a subscript denotes partial differentiation. The deviatoric part of the stress tensor, $\boldsymbol{\Sigma}$, is composed of a Newtonian component, corresponding to the Newtonian solvent, and a polymeric component, $\boldsymbol{T}$, corresponding to the solute. Thus,

$$\boldsymbol{\Sigma} = -P\boldsymbol{I} + \mu_s(\nabla \boldsymbol{U} + \nabla \boldsymbol{U}^t) + \boldsymbol{T}, \tag{2.2}$$

where P is the hydrostatic pressure, and t denotes matrix transposition. The constitutive equation for $\boldsymbol{T}$ is taken to correspond to the Oldroyd-B fluid, which can be written as (Bird, Armstrong & Hassager 1987):

$$\lambda(\boldsymbol{T}_{,T} + \boldsymbol{U} \cdot \nabla \boldsymbol{T} - \boldsymbol{T} \cdot \nabla \boldsymbol{U} - \nabla \boldsymbol{U} \cdot \boldsymbol{T}) + \boldsymbol{T} = \mu_p(\nabla \boldsymbol{U} + \nabla \boldsymbol{U}^t). \tag{2.3}$$

In the limit $\mu_s \to 0$, system (2.1)–(2.3) reduces to that corresponding to a Maxwell fluid. In the limit $\mu_p \to 0$, the Navier–Stokes equations are recovered. The problem is next examined in cylindrical polar coordinates (R, Θ, Z), with the usual notations for the velocity and stress components.

Thus, consider the axisymmetric flow of a viscoelastic fluid as it emerges from an annulus, as depicted in figure 1. The X-axis is directed vertically downward. The flow may be induced by an axial pressure gradient inside the annulus and/or simply by gravity. The emphasis in this study, however, is on the former configuration. The fluid is assumed to occupy a domain $\Omega(T)$ bounded by the free surface, $R = E(X, T)$, the wetted part of the cylindrical substrate, $R_S(X)$, and the annulus exit $X = 0$. Since the flow is axisymmetric, it will be examined in the (R, X)-plane, with $R = 0$ coinciding with the axis of the cylindrical substrate. The governing conservation and constitutive equations for axisymmetric flow of an Oldroyd-B fluid are given explicitly in Bird *et al.* (1987).

It is observed that the stress equations for $T_{R\Theta}$ and $T_{X\Theta}$ admit zero values unless these stress components do not vanish initially or at the boundary. In this work, homogeneous boundary and initial conditions will be assumed. The annulus gap, D, and the radius of the substrate at the annulus exit, $L \equiv R_S(X = 0)$, are taken as radial and axial scale lengths, respectively. Three dimensionless groups emerge for both Newtonian and non-Newtonian flows, namely, the modified Reynolds number, Re, the aspect ratio, ε, the Froude number, Fr, and the capillary number, which are explicitly written as:

$$Re = \frac{\rho V D^2}{L\mu}, \qquad \varepsilon = \frac{D}{L}, \qquad Fr = \frac{V}{\sqrt{gD}}, \qquad Ca = \frac{\mu V}{\sigma}, \tag{2.4}$$

where V is the mean flow velocity in the annulus, and is taken as the reference velocity. For a viscoelastic flow, two additional similarity parameters emerge, namely the Deborah number, De, and the solvent-to-solute viscosity ratio, Rv, this latter being related to the solvent-to-solution viscosity ratio, a. Thus,

$$De = \frac{\lambda V}{L}, \qquad Rv = \frac{\mu_s}{\mu_p}, \qquad a = \frac{\mu_p}{\mu} = \frac{1}{Rv + 1}. \tag{2.5}$$

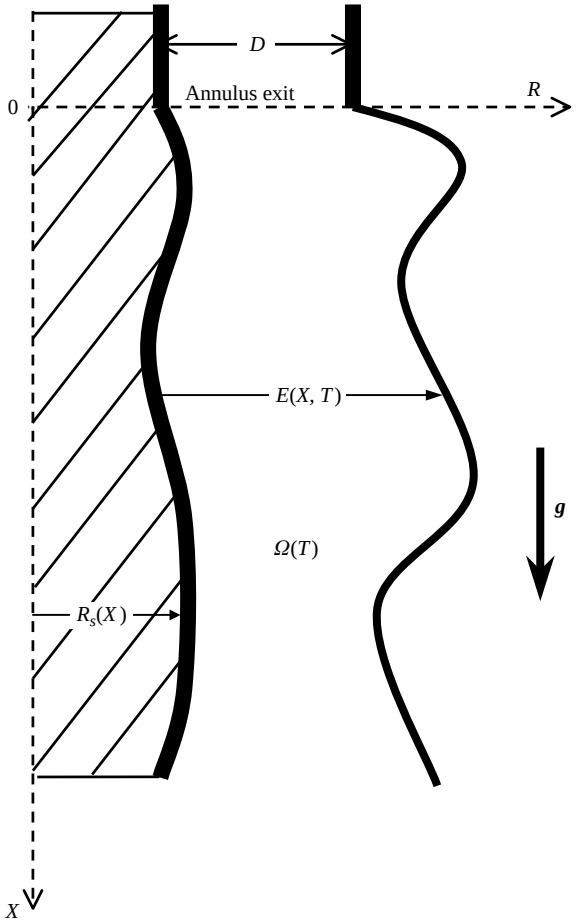

FIGURE 1. Schematic illustration of the axisymmetric flow of a viscoelastic fluid emerging from an annulus.

Alternatively, the elasticity number, defined here as $E = De/Re$, will also be used when highlighting the competition between inertial and elastic effects. Note that if the flow is gravity driven, the reference velocity will be taken as $V = \sqrt{gD}$. The film is assumed to be thin, with $\varepsilon \ll 1$. In this case, ε will be taken as the perturbation parameter to reduce the problem to the boundary-layer type.

The scaling of position coordinates, velocity and shear stress components is obvious, leading to

$$\left.\begin{gathered} x = \frac{X}{L}, \quad z = \frac{R-L}{D}, \quad t = \frac{V}{L}T, \quad u_x = \frac{U_X}{V}, \quad u_z = \frac{U_R}{V\varepsilon}, \\ p = \frac{L\varepsilon^2}{\mu V}P, \quad h = \frac{R_S - L}{D}, \quad \eta = \frac{E-L}{D} \\ \tau_{zx}(\tau_{xz}) = \frac{L\varepsilon}{\mu V}T_{RX}(T_{XR}),\ \tau_{zy}(\tau_{yz}) = \frac{L\varepsilon}{\mu V}T_{R\Theta}(T_{R\Theta}),\ \tau_{xy}(\tau_{yx}) = \frac{L\varepsilon}{\mu V}T_{X\Theta}(T_{\Theta X}). \end{gathered}\right\} \quad (2.6a)$$

The difficulty with the scaling of normal stress originates from the nonlinearities in the upper-convective terms. Generally, we may set

$$\tau_{xx} = \frac{L\varepsilon^{\alpha}}{\mu V} T_{XX}, \quad \tau_{yy} = \frac{L\varepsilon^{\beta}}{\mu V} T_{\Theta\Theta}, \quad \tau_{zz} = \frac{L\varepsilon^{\gamma}}{\mu V} T_{RR}, \tag{2.6b}$$

where α, β and γ are constants that are determined by ensuring the term balance in the conservation and constitutive equations. If these equations are cast in dimensionless form, and terms of $O(\varepsilon^2)$ and higher are excluded, then the reduced equations are obtained as in Appendix A.

Clearly, if all terms are accounted for in the axial momentum equation (A 2), and in analogy to the Newtonian limit, α should be set equal to 2. In this case, the axial normal stress, τ_{xx} does not depend strongly on the rate of axial elongation, $u_{x,x}$, as should be the case for shear dominated thin-film flow, but does not vanish because of the nonlinear coupling with shear effects. Similarly, all the terms in the radial stress equation (A 4) survive if $\beta = \gamma = 0$. This also ensures the survival of all the terms in equation (A 7), which governs τ_{zx}. In this case, the radial momentum equation (A 3) indicates that the pressure gradient in the radial direction $p_{,z} \sim O(\varepsilon^2)$. Therefore, and similarly to Newtonian film flow, the pressure dependence on film depth is negligible. Since there is no body force acting in the radial direction, $p = p(x, t)$. In this work, the inertia effect will be included in order to cover the widest flow range possible. In this case, the conservation and constitutive equations in Appendix A reduce to:

$$u_{x,x} + \varepsilon u_z + u_{z,z} = 0, \tag{2.7a}$$

$$Re(u_{x,t} + u_x u_{x,x} + u_z u_{x,z}) = -p_{,x} + \frac{Re}{Fr^2} + aRv(u_{x,zz} + \varepsilon u_{x,z}) + \tau_{xx,x} + \tau_{zx,z} + \varepsilon\tau_{zx}, \tag{2.7b}$$

$$p_{,z} = 0, \tag{2.7c}$$

$$De(\tau_{zz,t} + u_x\,\tau_{zz,x} + u_z\,\tau_{zz,z} - 2\tau_{zz}u_{z,z} - 2\tau_{zx}u_{z,x}) + \tau_{zz} = 2au_{z,z}, \tag{2.7d}$$

$$De(\tau_{yy,t} + u_x\,\tau_{yy,x} + u_z\,\tau_{yy,z} - 2\tau_{yy}u_z) + \tau_{yy} = \varepsilon a u_z, \tag{2.7e}$$

$$De(\tau_{xx,t} + u_x\,\tau_{xx,x} + u_z\,\tau_{xx,z} - 2\tau_{zx}u_{x,z} - 2\tau_{xx}u_{x,x}) + \tau_{xx} = 0, \tag{2.7f}$$

$$De(\tau_{zx,t} + u_x\,\tau_{zx,x} + u_z\,\tau_{zx,z} - \tau_{zz}u_{x,z} + \varepsilon\tau_{zx}u_z - \tau_{xx}u_{z,x}) + \tau_{zx} = au_{x,z}. \tag{2.7g}$$

Note that the continuity equation (2.7*a*) is used to substitute the term $-\tau_{zx}u_{x,x} - \tau_{zx}u_{z,z}$ in equation (A7) by the term $\varepsilon\tau_{zx}u_z$, which appears in equation (2.7*g*). It is observed that although the flow is decoupled from the azimuthal normal stress component, τ_{yy}, this stress component does not vanish. It is also assumed that no (wind) pressure acts on the fluid surface. For surface-pressure-driven flow, see Kriegsmann, Miksis & Vanden-Broeck (1998) and the references therein. In this case, and following the same scaling procedure as above, the dynamic condition in the tangential and normal directions leads, respectively, to

$$aRvu_{x,z}(x, z = \eta, t) + \tau_{xz}(x, z = \eta, t) = \tau_{xx}(x, z = \eta, t)\,\eta_{,x}(x, t), \tag{2.8a}$$

$$p(x, z = \eta, t) = -\frac{\varepsilon^3}{Ca}\eta_{,xx}. \tag{2.8b}$$

In dimensionless form, the kinematic condition becomes

$$u_z(x, z = \eta, t) = \eta_{,t}(x, t) + u_x(x, z = \eta, t)\eta_{,x}(x, t). \tag{2.9}$$

The no-slip and no-penetration boundary conditions at the cylindrical substrate are

$$u_x(x, z = h, t) = u_z(x, z = h, t) = 0. \tag{2.10}$$

The free surface is assumed to be fixed at the annulus exit so that

$$\eta(x = 0, t) = 1. \tag{2.11}$$

In addition, plug-flow conditions are assumed to hold at the annulus exit. As to initial conditions, the film layer is assumed to be of uniform thickness initially and at rest.

The present study is focused on the elastico-inertial range. The influence of surface tension tends to weaken for flow with dominant inertia and/or gravity. This has been particularly demonstrated for the flow of Newtonian films. Lee & Mei (1996) examined the formation of steady solitary waves on inclined Newtonian thin-film flow, and determined the dependence of the Weber number of different liquids on the Reynolds number for both small and large angles of inclination. They found that the surface tension effect decreases strongly with inertia. When cast in terms of the present similarity parameters, the Lee & Mei results show that the capillary number behaves roughly like $Ca \sim Re^2/\varepsilon$. This clearly suggests, from (2.8*b*), that the effect of surface tension is on the order of ε^4/Re^2. This argument may be extended to include turbulent flow of a thin film (Balmforth & Mandre 2004; Stansby & Feng 2005), or the limit of inviscid flow, such as the formation of tsunamis (Voit 1987), in which cases, surface-tension effects are clearly negligible. Omodei (1979) carried out a two-dimensional finite-element simulation of steady Newtonian jet flow. He found, for example, that the height of the free surface changes by 8% when the capillary number changes from 0.83 to infinity at a Reynolds number (based on channel exit half height) equal to 1, compared to a change in jet thickness of less than 1% when the Reynolds number is greater than 10. A further drop in capillary number is thus required to observe any palpable change in jet height at moderately large Reynolds number. However, further decrease in Ca is not realistic according to experiment. See, for instance, the early study by Goren & Wronski (1966) on capillary jet flow. The capillary number can be large for some (essentially) Newtonian fluid flow with high viscosity, such as the flow of polybutene oils. As an illustration, consider polybutene fluid with mean viscosity, $\mu = 80\,\mathrm{mPa\,s}$, density $\rho = 1200\,\mathrm{kg\,m^{-3}}$, and surface tension coefficient $\sigma = 50\,\mathrm{mN\,m^{-1}}$. The film is assumed to move at $12\,\mathrm{m\,s^{-1}}$ out of an annulus of 2 mm gap, on a substrate of radius $L = 20\,\mathrm{mm}$. In this case, $\varepsilon = 0.1$, $Re = 36$ and $Ca = 19.2$, making surface-tension effects negligible, and non-negligible inertia. This value of Ca is within the same order of magnitude as those encountered in polymer processing, such as the injection moulding of polybutene (Behrens *et al.* 1987).

Surface-tension effects are expected to be even less significant for typical polymeric film flow because of higher viscosity and lower surface-tension coefficient. In jet flow, for instance, polymer solution jets generally take longer to break up than Newtonian jets of comparable (shear) viscosity; sometimes, viscoelastic jets do not form droplets at all (Gordon, Yerushalmi & Shinnar 1973). Melt fracture occurs essentially in the absence of surface-tension effects for elastic fluids. Even weakly elastic fluids can lead to moderately large capillary numbers, such as 0.5 and 0.75% polyethylene oxides moving at a speed of $10\,\mathrm{m\,s^{-1}}$, with $Ca = 1.2$ and 11, respectively. Strongly elastic polyacrylamide solutions of 0.1 to 0.75% lead to corresponding Ca value in the range 16 to 600 (Middleman 1977). Boger fluids, such as the class of fluids considered in the present study, can also lead to large capillary number flow (Huzyak & Koelling 1997). For rimming flow, the scaling analysis of Fomin *et al.* (2003) also shows that surface-tension effects are negligible in this case.

In this work, it will be assumed that the Reynolds, Froude and Deborah numbers are all of order one, whereas $Ca = O(1/\varepsilon)$. The flow is therefore assumed to be inertia, elasticity and/or gravity dominated, and surface-tension effect will be neglected. The present work should be regarded as complementary to studies where surface-tension effects are dominant (see references in § 1). In this case, and similarly to Newtonian film flow, since p does not depend on z, the pressure must vanish everywhere to satisfy the zero-pressure condition (2.8*b*) at the film surface. From now on, the axial pressure gradient will be dropped from equation (2.7*b*).

2.2. *Solution procedure*

In the Newtonian literature, the equations for thin-film flow are generally solved by imposing a semi-parabolic profile for velocity and depth-averaging the equations across the thickness. This similarity approach leads to an exact formulation in the absence of inertia, and is commonly adopted in the presence of inertia, making it valid only to a flow at small Reynolds number or far from the (channel) exit (Watson 1964; Shkadov 1967; Prokopiou, Cheng, & Chang 1991). Clearly, this approach would not be adequate for viscoelastic flow given the strong nonlinearities stemming from both inertia and normal-stress effects. The key difficulty remaining, of course, is the explicit z-dependence of the velocity and stress components. Even if the x- and z-dependencies can be assumed to be decoupled, with possible use of a separation of variables type argument, the question remains as to the type of z-dependence. Formal treatments in the form of flow expansion in the z-direction were suggested (Zienkievicz & Heinrich 1979; Ruyer-Quil & Manneville 1998; Takeshi 1999). The current formulation closely follows and generalizes that of Zienkiewicz & Heinrich (1979), which emphasizes water flow over extended areas. However, in contrast to Zienkiewicz & Heinrich (1979), the radial (transverse) velocity component will not be neglected, and the variation in surface height with time and space will also be included.

The problem is first mapped onto the rectangular domain, then the flow variables are expanded in terms of polynomial shape functions in the z-direction, and the Galerkin projection method is applied to generate the equations that govern the expansion coefficients. A Lagrangian time-stepping implicit finite-difference approach is implemented for the solution of the equations that govern the expansion coefficients, coupled with a Runge–Kutta integration scheme along the flow direction. The solution procedure is similar to that developed previously for the two-dimensional coating flow of Newtonian (Khayat & Welke 2001) and generalized Newtonian fluids (Kim & Khayat 2002). In the present case, the methodology is even more involved, but only a summary will be given. System (2.7) is reduced to a transient one-dimensional problem by expanding the velocity and stress components in terms of orthonormal modes in the radial direction. The axial velocity component, u_x, and the normal stress components, τ_{xx} and τ_{zz}, and the shear stress component, τ_{xz}, are represented in terms of orthonormal shape functions, $\phi_i(\xi)$, $\psi_i(\xi)$ and $\theta_i(\xi)$, as follows:

$$\left.\begin{aligned} u_x(x,z,t) &= \sum_{i=1}^{M} U_i(x,t)\phi_i(\xi), \quad \tau_{xz}(x,z,t) = \sum_{i=1}^{M} S_i(x,t)\psi_i(\xi), \\ \tau_{zz}(x,z,t) &= \sum_{i=1}^{M} R_i(x,t)\theta_i(\xi), \quad \tau_{xx}(x,z,t) = \sum_{i=1}^{M} Q_i(x,t)\theta_i(\xi), \end{aligned}\right\} \tag{2.12}$$

where M is the number of modes, $U_i(x,t)$, $R_i(x,t)$, $Q_i(x,t)$ and $S_i(x,t)$ are unknown coefficients, and $\xi = (1/\Delta)(z - \Sigma/2)$ is the mapping from $z \in [h, \eta]$ to $\xi \in [-1/2, +1/2]$.

Here, $\Sigma = \eta + h$ and $\Delta = \eta - h$. In addition to the orthonormality condition, the shape functions must satisfy various boundary conditions, some of which are not obvious. Guidance may be taken from limit flow configurations, particularly the steady flow on straight substrate due to gravity, and, more importantly, the limit of Newtonian film flow, which must be recovered by the viscoelastic formulation as $Rv \to \infty$. The difficulty for viscoelastic flow originates from the fact that, in contrast to Newtonian flow, the shear stress does not simply and necessarily vanish at the free surface. This difficulty is reflected in condition (2.8*a*), and the fact that there are no separate boundary conditions on shear and normal stresses. However, one way to satisfy condition (2.8*a*) and recover the Newtonian limit is simply to set both shear and normal stresses equal to zero at the free surface. Thus,

$$\langle \phi_i \phi_j \rangle = \delta_{ij}, \qquad \phi_i\left(\xi = -\tfrac{1}{2}\right) = \phi_i'\left(\xi = +\tfrac{1}{2}\right) = 0, \tag{2.13a}$$

which satisfy condition (2.10). Here δ_{ij} is the Kronecker delta, and $\langle\ \rangle$ denotes the integral over the interval $\xi \in [-1/2, +1/2]$. Noting that ψ_i must be one order less than ϕ_i, we have

$$\langle \psi_i \psi_j \rangle = \delta_{ij}, \qquad \psi_i\left(\xi = \tfrac{1}{2}\right) = 0. \tag{2.13b}$$

The boundary conditions for θ_i are less obvious. However, the normal stress is expected to behave predominantly like the square of shear stress in the present shear-dominated flow. At the free surface, both the normal and shear stresses are taken to vanish. At the substrate, we can expect the shear stress to reach a maximum. In this case,

$$\langle \theta_i \theta_j \rangle = \delta_{ij}, \qquad \theta_i\left(\xi = +\tfrac{1}{2}\right) = \theta_i'\left(\xi = -\tfrac{1}{2}\right) = 0. \tag{2.13c}$$

The first three modes for the shape functions are explicitly given in Appendix B. The radial velocity component, u_z, is determined by integrating the continuity equation (2.7*a*) to give

$$\begin{aligned} u_z(x,z,t) = {} & \Delta \sum_{k=1}^{M} [\varepsilon \Delta (F_k \xi - G_k) - F_k] U_{k,x} \\ & - \sum_{k=1}^{M} \left[\Delta_{,x} (F_k - \phi_k \xi) - \frac{\sum_{,x}}{2} \phi_k - \varepsilon \Delta \Delta_{,x} (F_k \xi - 2G_k) + \varepsilon \Delta \frac{\sum_{,x}}{2} F_k \right] U_k, \end{aligned} \tag{2.14}$$

where $F_i(\xi) = \int_{-1/2}^{\xi} \phi_i(\xi)\, \mathrm{d}\xi$ and $G_i(\xi) = \int_{-1/2}^{\xi} \xi \phi_i(\xi)\, \mathrm{d}\xi$.

Expression (2.14) allows the elimination of the radial velocity component. The mean values of the axial and radial velocity components are denoted by $U(x,t)$ and $W(x,t)$, respectively, whereas those of shear, radial and axial normal stress components are denoted by $S(x,t)$, $R(x,t)$ and $Q(x,t)$, respectively. The mean primary normal stress difference is then given by $N(x,t) = Q(x,t) - R(x,t)$ In this case, the kinematic equation may be rewritten as:

$$(1 + \varepsilon \eta)\, \eta_{,t} = -(\eta_{,x} - h_{,x})\, U - (\eta - h)\, U_{,x} = -\Delta_{,x}\, U - \Delta U_{,x}\,. \tag{2.15}$$

Similarly to Newtonian and generalized Newtonian flows (Khayat & Welke 2001; Kim & Khayat 2002), it is found that any arbitrary number of modes can be introduced, each satisfying the boundary and orthonormality conditions, but reasonable accurate radial distributions can be obtained with $M = 2$ or 3. A hierarchy of equations are obtained for the coefficients, $U_i(x,t)$, $Q_i(x,t)$, $R_i(x,t)$ and $S_i(x,t)$, when expansions

(2.12) and (2.14) are substituted into equations (2.7), which are then multiplied by the appropriate shape functions and integrated over $\xi \in [-1/2, +1/2]$. The resulting system of $4M + 1$ partial differential equations in the (x, t) domain are shown in Appendix C, and are then solved using an implicit finite-difference discretization in time and sixth-order Runge–Kutta integration scheme in x.

3. Discussion and results

The formulation and numerical implementation above is now applied to examine the steady and transient viscoelastic film flow emerging from the annulus, as illustrated schematically in figure 1. The influence of fluid elasticity is examined for moderately low Reynolds number so as not to make inertia dominant. The physical domain of the fluid is assumed to extend from $x = 0$ to $x \to \infty$, but the domain of computation will be restricted to $x \in [0, 10]$. The influences of inertia, aspect ratio, substrate topography and gravity are also investigated. Calculations are based on $M = 3$ unless otherwise specified.

It will be helpful to consider limit flow cases where analytical expressions can be obtained. The depth-averaged equations, which correspond to $M = 1$, are amenable to analytical manipulation. For simplicity, the discussion will be limited to steady two-dimensional flow ($\varepsilon = 0$) over a straight cylinder ($h = 0$). In this case, the depth-averaged x-momentum, axial and radial normal stress, and shear stress equations reduce, respectively, to:

$$ReUU_{,x} = \frac{Re}{Fr^2}C_1 + a\,RvC_2U^3 + C_3Q_{,x} + C_4\frac{U_{,x}}{U}Q + C_5US, \tag{3.1a}$$

$$De\left[UR_{,x} + C_6RU_{,x} + C_7S\frac{U_{,x}^2}{U^2} + C_8S\frac{U_{,xx}}{U}\right] + \alpha R = aC_9U_{,x}, \tag{3.1b}$$

$$De(UQ_{,x} + C_{10}QU_{,x} + C_{11}U^2S) + \alpha Q = 0, \tag{3.1c}$$

$$De\left[US_{,x} + C_{12}Q\frac{U_{,x}^2}{U^2} + C_{13}Q\frac{U_{,xx}}{U} + C_{14}U^2R\right] + \beta S = aC_{15}U^2. \tag{3.1d}$$

These equations must be solved subject to:

$$U(x = 0) = 1, \qquad Q(x = 0) = R(x = 0) = S(x = 0) = 0. \tag{3.2}$$

In this case, the film height and mean depthwise velocity component are given in terms of the mean streamwise velocity component through

$$\eta(x) = \frac{1}{U(x)}, \qquad W(x) = C_{16}\frac{U_{,x}}{U} = -C_{16}\frac{\eta_{,x}}{\eta}. \tag{3.3}$$

The constants α, β and $C_1, \ldots, C_{16}$ are introduced in Appendix D. Analytical solutions will be discussed for a Newtonian flow, and viscoelastic flows with dominant inertia and gravity. In general, the depth-averaging formulation is expected to hold reasonably well for the flow far from the annulus exit where no rapid variation in velocity and stress occur.

3.1. *Influence of elasticity and retardation*

The influence of fluid elasticity can be examined by either varying Rv or De. The overall influence of elasticity on steady film flow on a straight substrate is reported in figure 2, where the steady film profile, $\eta_s(x)$, mean radial velocity, $W_s(x)$, mean polymeric primary normal stress difference, $N_s(x)$, and mean polymeric shear stress,

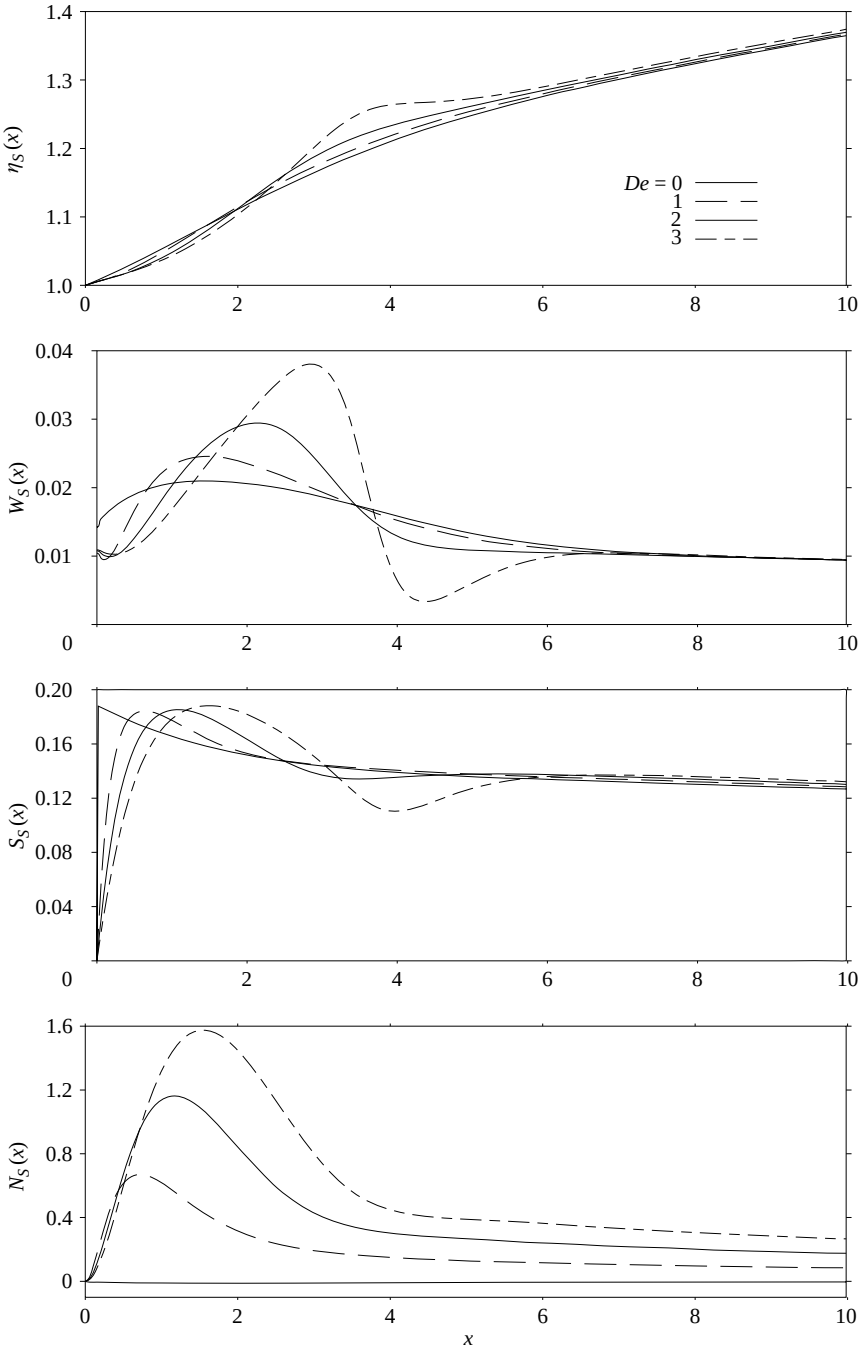

FIGURE 2. Influence of elasticity on steady-state film height, mean radial velocity component, shear stress and normal stress, in the absence of gravity ($1/Fr = 0$). $Re = 100$, $Rv = 1$, $\varepsilon = 0.1$ and $De \in [0, 3]$.

$S_s(x)$, are shown for $De \in [0, 3]$, $Rv = 1$, $Re = 100$ and $\varepsilon = 0.1$. The mean axial velocity, $U_s(x)$, is essentially a mirror image of the film height as a result of mass conservation, and will therefore not be explicitly considered. At small Deborah

number, the film exhibits a swell near the annulus exit, which is typical of both Newtonian and viscoelastic fluids, and the film thickness increases monotonically with position. The radial flow velocity exhibits a maximum, which also corresponds, expectedly, to a maximum in shear stress. The flow conditions appear to be little affected by elasticity far downstream. The radial flow is particularly strong near the annulus exit, but essentially vanishes shortly downstream. At some distance from the annulus exit ($x > 5$), the film thickness increases linearly with distance with a slope that is independent of De. Both the radial velocity and stress components approach relatively constant levels, with considerable weakening of radial flow. It is observed that although shear effects are evidently strong near the annulus exit, their level becomes essentially the same regardless of fluid elasticity. In contrast, elongation effects depend strongly on De. This dependence of $N_s(x)$ on De is, in fact, linear, similar to that for a flow in a duct, as velocity gradients tend to diminish significantly far downstream. In this case, the flow kinematics is essentially that of Newtonian flow. In the case of very small Deborah number ($De = 0$ in this case), while the normal stress increases smoothly near the annulus exit ($x = 0$), the shear stress experiences a sudden jump. A jump in polymeric stresses is expected in the limit $De \to 0$ given the singularity of the constitutive equations in this limit. See, for instance, Khayat & Pan (2004) for a multiple-scale analysis for the viscoelastic free-surface flow inside a thin channel. However, in the present problem, the singularity is felt only in the shear stress as a result of strong shearing near the annulus exit, with a jump estimated at $\tau_{zx,x} \approx au_{x,z}/De$, as equation (2.7$g$) suggests. The absence of elongational term in the normal stress equations prohibits a similar singular behaviour in $N_S(x = 0)$. The normal stress equations, (2.7e, f), are identically satisfied for vanishingly small normal stress and rate of strain.

Beyond a critical value, De_c, of the Deborah number (here $De_c \approx 0.5$), the film profile exhibits a wavy structure, which tends to dampen with x. This waviness is particularly obvious here for $De = 3$. Although the normal stress profiles are not affected qualitatively by the level of elasticity, the profiles of the radial velocity and shear stress exhibit a minimum when the film becomes wavy. More importantly, and this is particularly obvious from the W_s profiles, a steep gradient develops between the two extrema, which evolves toward a discontinuity or shock as De increases further ($De > 3$). This response is similar to that encountered under steady-state conditions for gravity-driven flow (Kriegsmann *et al.* 1998). This signals, in reality, the breakdown or rupture of the film. The spatial waviness is generally associated with temporal overstability, which is typically expected for highly elastic fluids. The spatial instability is difficult to predict in most viscoelastic studies involving free-surface flow because it is associated with steep strain rate, as illustrated in figure 2.

The link between shock formation and film rupture is invoked here because of the similarity of viscoelastic film flow with solid deformation (Middleman 1987; Tanner 1999). We may then suspect that, unlike Newtonian films, a viscoelastic film need not reach zero or negligible thickness to rupture. However, a viscoelastic rupture is not expected to be brittle; some necking down must still occur before rupture, similarly to ductile fracture. Rupture occurs in solids when the stress exceeds a critical level. Analogously, melt fracture occurs in viscoelastic fluids once the wall shear stress (or, equivalently, the Deborah or Weissenberg number) exceeds a critical value. The onset of waviness predicted in figure 2 is of course reminiscent of the onset of melt fracture in film extrusion/casting. The waviness also correlates with the onset of buckling instability predicted in viscoelastic film flow (Kumar & Graham 2000). For a Newtonian film flowing on a rigid substrate, the main rupture mechanism

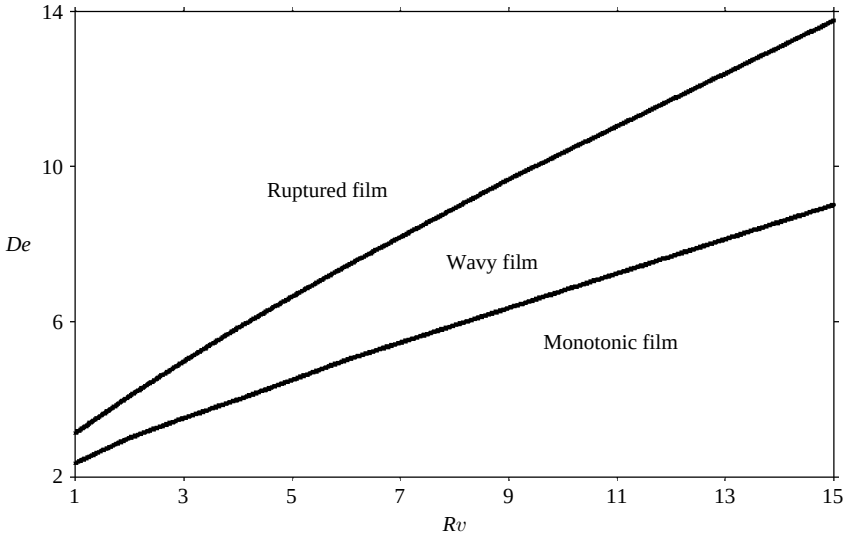

FIGURE 3. Dependence of the critical Deborah number on the viscosity ratio for the onset of steady film waviness and rupture, in the absence of gravity ($1/Fr = 0$). $Re = 100$ and $\varepsilon = 0.1$.

is the combined effect of shearing and surface-tension. For a viscoelastic film, the combination of shearing and extension is expected to play the dominant role in film rupture. Extensional flow obviously results from normal stress (elastic) effects, and is expected to increase as film waviness increases. As the shock forms in flow velocity (reflecting infinite shear rate), the film experiences a significant increase in both shear and normal stress (eventually to infinity), but especially in normal stress as this latter grows as the square of shear rate, while shear stress remains essentially proportional to shear rate. Close to shock formation, normal stress is expected to exceed a critical value, which, similarly to solid fracture, should unavoidably lead to film rupture.

In this work, shock formation is assumed to be closely associated with film rupture. To our knowledge, this association has not been made previously in the literature. However, for filament jet flow (for instance) the maximal strain rate occurs during the final breakup of the filament (Christanti & Walker 2001). Shock formation is examined further for $Re = 100$ as a function of the viscosity ratio. Figure 3 illustrates the dependence of the threshold Deborah numbers on viscosity ratio for the onset of spatial waviness and film rupture. The two delimiting De curves are monotonic, with linear dependence on Rv for large viscosity ratio. The margin of wavy film flow tends to widen with Rv. Figure 2 shows clearly that spatial waviness is of secondary nature as the oscillation appears in the form of modulation around the mean free-surface level. The waviness is thus suspected to result from severe coupling between normal stress and flow kinematics, and may thus not be captured in a formulation that is only weakly nonlinear. Valuable lessons have already been learned from the flow of a thin Newtonian film. In that case, Watson's similarity solution serves as a reference against which approximate solutions can be compared. It was shown, in particular, that the depth-averaging formulation is not satisfactory for Newtonian flow, even for flow with moderate inertia. For strongly nonlinear flow, a Galerkin projection formulation, similar to the one adopted here for the viscoelastic problem, is required, and leads to excellent agreement with Watson's similarity solution (Kim & Khayat 2002).

Additional insight is gained by examining the solution to the depth-averaged equations (3.1) in the absence of gravity. Since the current results are reported for moderately large Reynolds number, a perturbation expansion will be carried out in terms of the small parameter $1/Re$. To leading order in $1/Re$, the flow from equations (3.1) is given by

$$\left.\begin{aligned} \eta_s(x) = U_s(x) = 1, \quad W_s(x) = R_s(x) = 0, \quad S_s(x) = \frac{aC_{15}}{\alpha}\left(1 - \mathrm{e}^{-\alpha x/De}\right), \\ N_s(x) = -aDeC_{11}C_{15}\left[1 + \frac{\alpha\beta}{\alpha - \beta}\left(\frac{\mathrm{e}^{-\alpha x/De}}{\alpha} - \frac{\mathrm{e}^{-\beta x/De}}{\beta}\right)\right], \end{aligned}\right\} \tag{3.4}$$

which reveals that the stress components decay monotonically with x. Both normal and shear stresses scale linearly with the solute-to-solvent viscosity ratio, a. At large x, the shear stress approaches a level independent of fluid elasticity, whereas the normal stress approaches a level that is proportional to De. These observations are qualitatively consistent with the results in figure 2. More generally, it is clear that inertia tends to weaken the maximum in shear and normal stresses, to eventually lead to monotonic growth. Thus, a film flowing at relatively higher rate or possessing relatively smaller viscosity tends to rupture further downstream. For a typical viscoelastic film flow, inertia tends to be moderate, and the film is likely to rupture near the annulus exit. The solution to $O(1/Re)$ shows that the film height does not possess an extremum, which thus excludes the onset of spatial waviness. It is therefore concluded that, in contrast to the current formulation, the depth-averaged equations cannot support the onset of spatial waviness. It is emphasized that the weakness of the depth-averaged equations is the decoupling resulting from the assumption of similarity profile across the film.

Consider now transient flow. Two contrasting flow limits will be examined in order to illustrate the influence of elasticity, namely the case of a Newtonian fluid, and that of an upper-convected Maxwell fluid. The Newtonian flow limit is recovered by setting $Rv \to \infty (aRv = 1)$. Figure 4 shows the evolution of the Newtonian film height, $\eta(x, t)$, as well as that of the mean radial velocity component, $W(x, t)$, for a flow at $Re = 100$ and $\varepsilon = 0.1$. A three-dimensional perspective is also shown. The figure shows the film height at equal time intervals, including the (flat) initial and steady-state profiles. The film height displays a maximum, which propagates downstream with time, exhibiting a wavelike structure. The surface wave widens with time as the film thickens everywhere. There is lack of symmetry with respect to the wave crest as a result of high inertia. The steady state is swept closely by the wave tail, but the film surface is always below the steady state. Eventually, the steady state is reached. The mean radial flow reaches a maximum at the crest of the surface wave, but the maximum weakens with time as the flow approaches the steady state.

In the presence of elasticity, the flow response can be dramatically different. Figure 5 shows the flow response for a highly elastic fluid. In this case, $Re = 100$, $\varepsilon = 0.1$, $Rv = 0$ and $De = 2$. There is a tendency for the film height to propagate downstream in the form of a solitary wave, but, in contrast to Newtonian flow, the wave tends to simultaneously move upward, exceeding the steady state, and asymptotically levelling off further downstream. With time, the film height experiences a sharp drop downstream as the wave steepens. The drop is a reflection of strong elongational flow or normal stress as in converging/diverging flow. There is simultaneously a strong radial normal stress. The radial flow velocity increases overall in strength as the fluid moves downstream and reaches a maximum at the crest of the surface wave. As the free

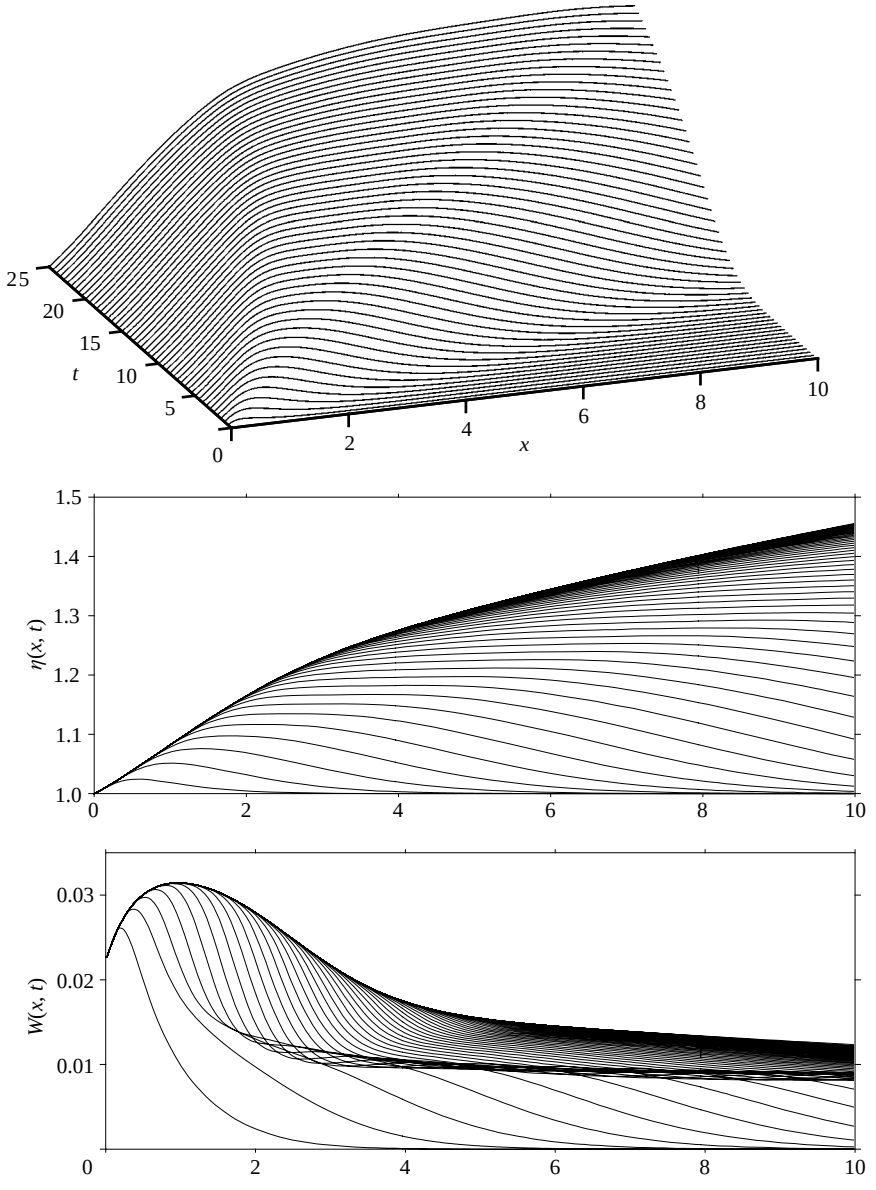

FIGURE 4. Transient flow response for a Newtonian fluid, in the absence of gravity ($1/Fr = 0$). $Re = 100$ and $\varepsilon = 0.1$. The figure shows the evolution of the film height and mean radial velocity. A three-dimensional perspective is also shown.

surface deforms further, W exhibits a maximum at the tail of the wave, a minimum at the crest, and a relatively weak maximum ahead of the crest, to then asymptotically vanish downstream, where the film is practically of constant thickness. There is considerable gain in strength in radial flow with time, with W reaching a third of the axial flow in magnitude. However, the steady radial flow is relatively weak. The significance of the radial flow is further appreciated when the entire flow field is examined (not shown), which indicates clearly the sudden change in direction that the radial flow takes below the crest, where a strong radial flow develops near the

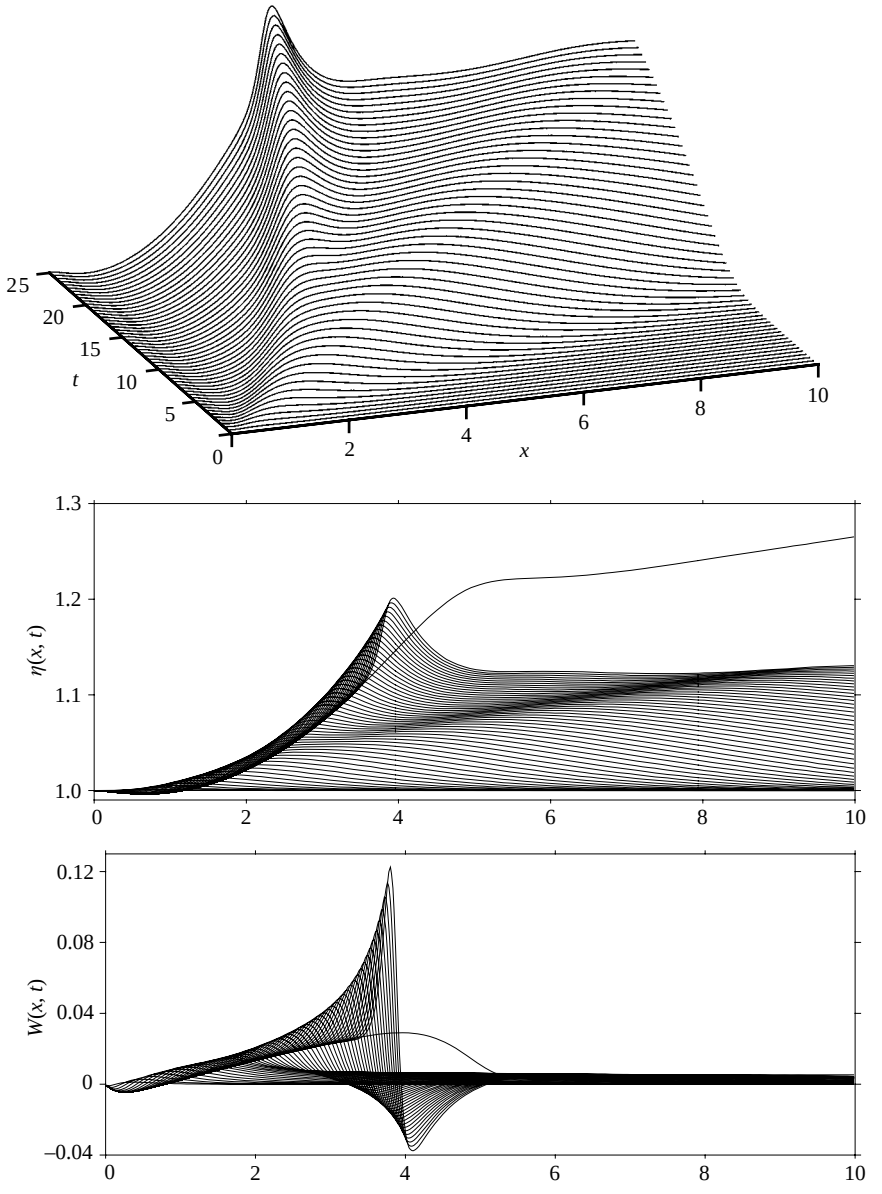

FIGURE 5. Transient flow response for a highly viscoelastic fluid, in the absence of gravity ($1/Fr = 0$). $Re = 100$, $Rv = 0$, $\varepsilon = 0.1$ and $De = 2$. The figure shows the evolution of the film height and mean radial velocity. A three-dimensional perspective is also shown.

substrate, along with a strong inward flow below the wave crest. It is important to note that the radial flow is not negligible as the long-wave approximation suggests (Takeshi 1999). The strong jump in radial flow depicted from figure 5 clearly reflects shock formation, and simultaneously signals the rupture of the film. Unlike the case of a Newtonian fluid (see figure 4), there is strong movement towards the substrate ($W < 0$). At any time, the trailing edge of the surface wave embraces closely the steady-state profile. There is additional symmetry breakup in the wave shape as a result of the combined effect of both inertia and normal stress. The question as

to whether the steady-state profile is ever reached over the long time is obviously important to address. The current thin-film results clearly indicate that the steady profile will never be reached for a highly elastic fluid. Additional mechanisms are required to halt the wave growth, such as surface-tension and/or gravity effects (Kalliadasis & Chang 1994). However, surface-tension effects are probably negligible for highly elastic polymeric films flowing with high inertia. It is thus expected that viscoelastic films experience pronounced spatial (and temporal) fluctuation, resulting in film rupture, similarly to the breakdown of polymeric flows in other processes such as melt fracture (Tanner 1999). The wave growth displayed in figure 5 is not the result of numerical instability; rigorous convergence and stability criteria have been applied to ensure numerical accuracy (see Khayat & Welke 2001; Khayat & Kim 2002; Kim & Khayat 2002). The steady state is simply unconditionally unstable (to both infinitesimal and finite disturbances). The viscoelastic flow equations, especially the boundary-layer equations (2.7) and (2.9), are hyperbolic, and the wavelike behaviour is effectively the result of the hyperbolic nature of the thin-film equations. The origin of wave growth and the role of initial conditions were examined previously for a Newtonian fluid (Khayat & Kim 2002).

3.2. *Role of inertia and gravity in viscoelastic film flow*

The forces of inertia, gravity and normal stress compete in an intricate and significant manner. Obviously, for typical polymeric flow, inertia tends to be less dominant, leaving normal stress effects to play an even more dominant role than demonstrated above. An interesting question is whether a flow with both high normal stress and inertia behaves similarly to a flow with both low normal stress and inertia. In other words, is it only a matter of relative dominance (of inertia relative to normal stress effect) that is of significance to film flow? If this is the case, there should be only one similarity parameter in the problem; the elasticity number should replace both the Deborah and Reynolds number (see below). The flow at both moderately large Reynolds and Deborah numbers has already been examined above (see figure 2). Consider now the influence of inertia for a flow at smaller Deborah number. Figure 6 illustrates the flow response for $De = 0.5$, $Rv = 1$, $\varepsilon = 0.1$, and $Re \in [20, 100]$, in the absence of gravity. A significant difference is found, at least in appearance, between the flow with both high elasticity and inertia (figure 2) and the flow with both low elasticity and inertia (figure 6). In the latter case, for relatively low inertia (see the curves corresponding to $Re = 20$ in figure 6), the surface height experiences a sudden change in slope near the exit. Simultaneously, there is a strong maximum in velocity and stress that is present at the point of transition, followed by a weak minimum. This behaviour is reminiscent of continuous phase transition (Reichl 1984), where, similarly to the film height, the Gibbs free energy is continuous against temperature, but its slope changes rapidly. This in turn leads to a peaking in the heat capacity at the transition point, similarly to the peaking in velocity and stress here. In the present case, the slope $\mathrm{d}\eta_s/\mathrm{d}x$ behaves like the entropy. As Re increases, the transition in slope subsides, leading to a smoother monotonic increase in film height. There is symmetry around the maximum in velocity and stress for a flow with weak inertia, resulting from the weak symmetry-breaking convective terms compared to figure 2. Closer comparison between figures 2 and 6 hints at a similarity in the flow. This is particularly striking when the curves corresponding to $De = 3$ in figure 2 ($Re = 100$) are compared to the curves corresponding to $Re = 20$ in figure 6 ($De = 0.5$). The similarity in behaviour becomes evident stretching the x values in figure 6. Note in this case that the elasticity number is roughly the same, 0.03 compared to 0.025. The

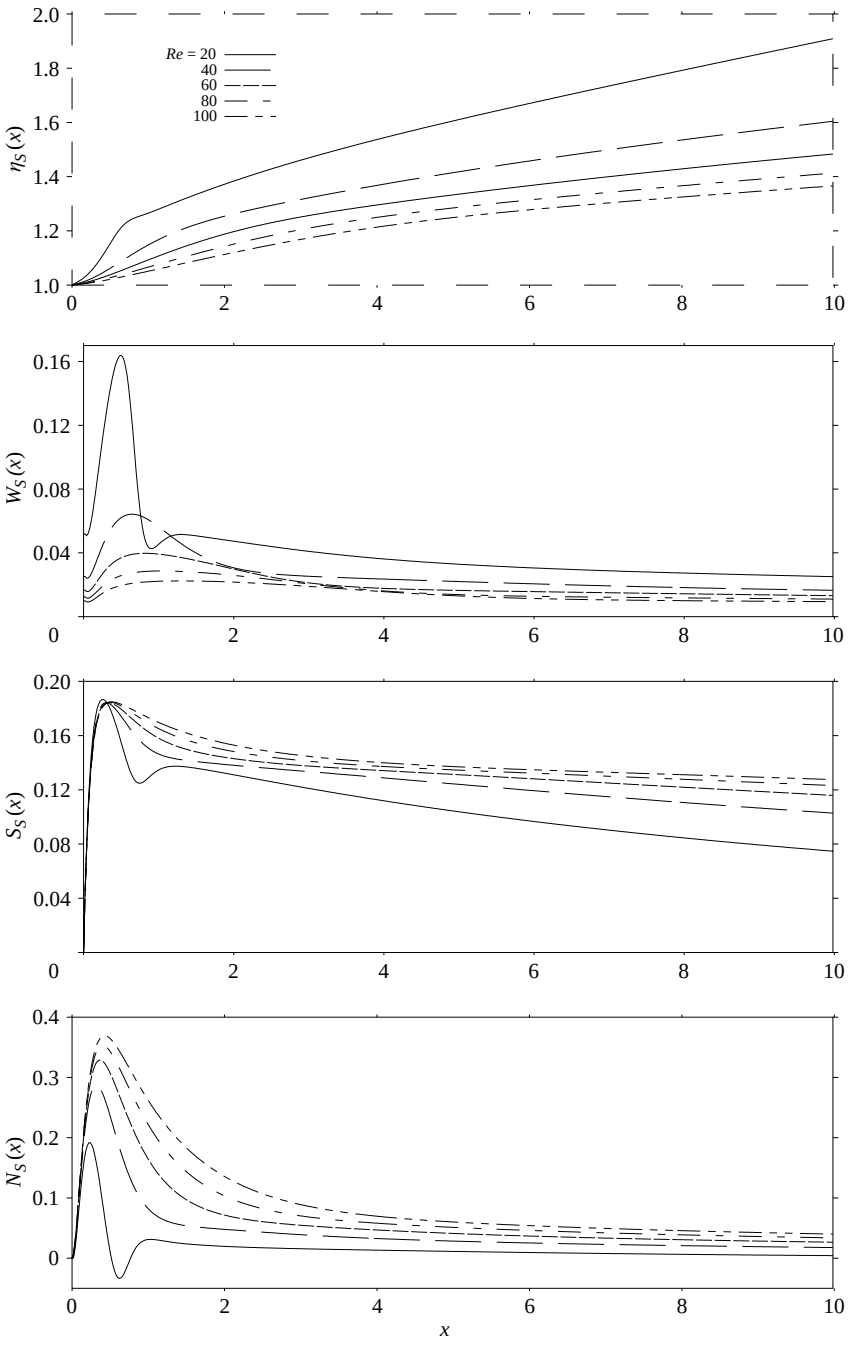

FIGURE 6. Influence of inertia on steady-state film height, mean radial velocity component, shear stress and normal stress for a viscoelastic fluid, in the absence of gravity ($1/Fr = 0$). $De = 0.5$, $Rv = 1$, $\varepsilon = 0.1$ and $Re \in [20, 100]$.

issue of similarity and scaling will be revisited below after considering the effects of gravity on the flow.

Further insight into the role of inertia is now gained by inspecting the solution of the depth-averaged equations (16) for a Newtonian fluid. In this case, the height and

mean radial velocity component reduce to:

$$\eta_s(x) = 1 - C_2\frac{x}{Re}, \quad W_s(x) = \frac{C_2C_{16}}{Re - C_2x}. \tag{3.5}$$

Clearly, the film thickness grows linearly with x, with a slope equal to $-C_2/Re = 2.33/Re$. This linear behaviour and the dependence on the Reynolds number are similar to the film profiles shown in figure 6. The slope is overestimated by equation (3.5) when compared to the value of $1.83/Re$ predicted by Watson's (1964) similarity y solution. Clearly, the film at lower Reynolds number tends to grow more rapidly near the exit; the lack of inertia prohibits the film from advancing downstream. In the limit of creeping flow, the fluid accumulates near the annulus exit and does not move. This is a singular limit for thin-film or boundary-layer flow (see equation (2.2)).

So far, results were reported in the absence of gravity. In contrast to two-dimensional flow, gravity acts in the direction of axial flow, which makes the gravity term easier to handle as it is decoupled from the surface height. However, the effect of gravity can be significant even though it is present as a constant source term in equation (2.7*b*). Some insight may be preliminarily gained by examining two-dimensional steady-state flow using the depth-averaged equations (3.1). In particular, two limit flows can be recovered analytically, namely the flow with high inertia, and Newtonian flow. For a viscoelastic fluid at high Reynolds number,

$$\eta_s(x) = \frac{1}{\sqrt{\dfrac{2C_1}{Fr^2}x + 1}}, \quad W_s(x) = \frac{C_1C_{16}}{2C_1x + Fr^2}, \tag{3.6}$$

indicating that the film height (velocity) decreases (increases) monotonically with position. For a Newtonian fluid at any Reynolds number, the film is dictated by the equation:

$$\frac{\mathrm{d}\eta_s}{\mathrm{d}x} = -\frac{C_2}{Re}\left(1 + \frac{C_1Re}{C_2Fr^2}\eta_s^3\right) = \frac{2.33}{Re}\left(1 - \frac{Re}{3.6Fr^2}\eta_s^3\right). \tag{3.7}$$

The presence of gravity for a viscous fluid generally forces the free surface to deviate from the linear growth in (3.5). The vanishing of the slope signals either a reversal from growth to decay near the annulus exit, or a levelling in film height far downstream. Hence, at a critical Froude number, $Fr_c = \sqrt{Re/3.6}$, the slope at the annulus exit is zero, and remains zero for $x > 0$. In this case, viscous and gravity forces are in balance. For $Fr > Fr_c (Fr < Fr_c)$, the surface slope far downstream is positive (negative). Consequently, the film height decreases (increases) with x until it levels off at a certain position, $x = x^*$, where the film thickness remains constant further downstream ($x > x^*$), with corresponding film height $\eta_s^* \equiv \eta_s(x^*) = \sqrt[3]{3.6Fr^2/Re}$. This prediction should also hold for a viscoelastic fluid since the flow kinematics is essentially independent of the Deborah number far from the exit.

The observations based on expressions (3.6) and (3.7) are expected to hold reasonably for axisymmetric flow, especially when the aspect ratio, ε, is very small. Figure 7 illustrates typically the influence of gravity on steady-state flow with high inertia, for $Re = 100$, $Rv = 1$, $\varepsilon = 0.1$, $De = 2.5$ and $1/Fr \in [0, 0.5]$. The critical Froude number for reversal from growth to decay in film height is estimated from figure 7 to be $Fr_c \approx 6$, which is slightly higher than that corresponding to two-dimensional Newtonian flow ($Fr_c = 5.22$). When the gravity effect is dominant, η_s decreases at a rate essentially equal to the prediction of equation (3.7). In this case, the critical surface level is estimated from two-dimensional flow to be approximately $\eta_s^* = \sqrt[3]{0.036Fr^2}$. For

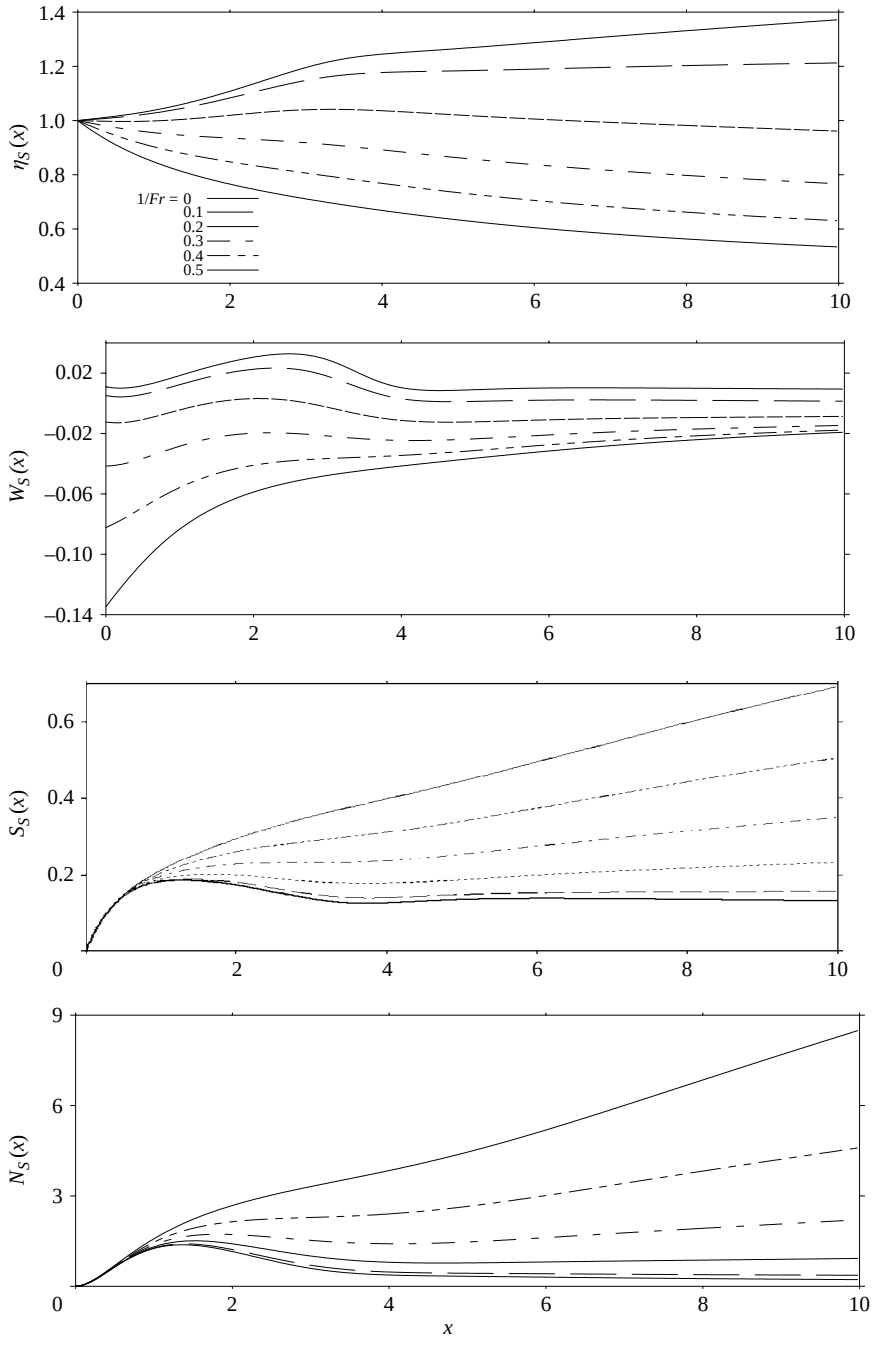

FIGURE 7. Influence of gravity on steady-state film height, mean radial velocity component, shear stress and normal stress, for a viscoelastic fluid with high inertia. $Re = 100$, $Rv = 1$, $\varepsilon = 0.1$, $De = 2.5$ and $1/Fr \in [0, 0.5]$.

a flow with relatively weak gravity, this approximation is expected to be poor given the relatively strong elastic effect. Indeed, for $1/Fr = 0.1$, the film height is 1.21, with an overestimate of 1.44 by the two-dimensional Newtonian prediction (3.7). Figure 7 indicates that the mean radial flow is strongly affected by gravity near the annulus

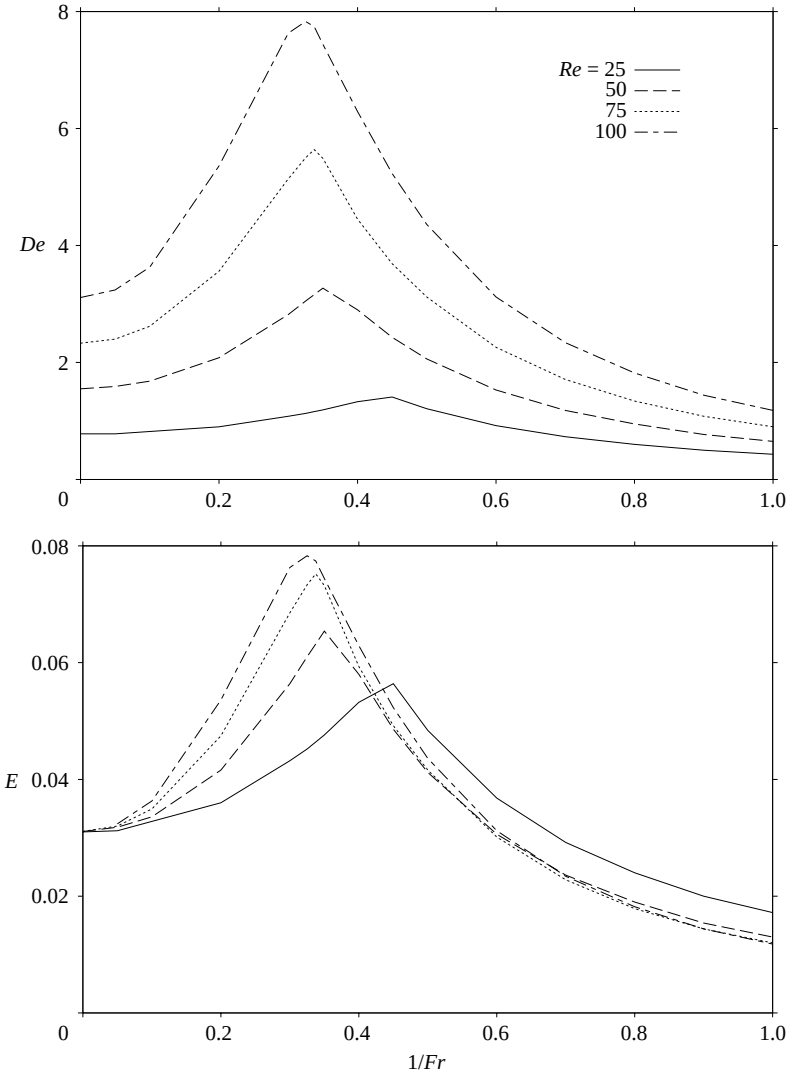

FIGURE 8. Dependence of the critical Deborah and elasticity numbers on gravity and inertia for the onset of steady film rupture. $Rv = 1$, $\varepsilon = 0.1$ and $Re \in [20, 100]$.

exit while the shear and normal stress are not. Both velocity and stress display an overshoot when gravity is weak, but tend to increase monotonically with position when gravity is strong. In this case, elongational effects are strong as a result of film contraction. The flow with relatively high inertia and gravity is typically reflected by the profiles corresponding to $1/Fr = 0.5$ in figure 7. Indeed, expressions (3.6) appear to be excellent approximations for this case, giving very close estimates of $\eta_s(x = 10) = 0.48$, $W_s(x = 10) = -0.022$ to those in the figure.

It is then clear that the contraction due to gravity increases normal stress effects, which in turn are expected to play a prominent role in causing film rupture. The interplay between gravitational and elongational effects (as well as those of inertia) in this case is, however, not obvious. Figure 8 shows the dependence of the critical

level of fluid elasticity for film rupture on gravity, for various levels of inertia. The critical Deborah and elasticity numbers are plotted against $1/Fr$ for $Rv = 1$, $\varepsilon = 0.1$ and $Re \in [25, 100]$. Several important observations are inferred from figure 8. A low-inertia film tends to rupture at lower Deborah number, which is essentially independent of gravity. More importantly, and by extrapolation, the film appears to be uniformly unstable in the (singular) limit of zero Reynolds number. There is a maximum in De_r, which strengthens with Re. Thus, there is an optimum level of gravity that exists, which varies slightly with Re, at which the film is most stable. The critical Deborah number increases linearly in the absence of gravity, which explains the independence of E on Re in this case. This is almost the case also for a strong gravitational effect, where the E *vs.* $1/Fr$ curves tend to collapse onto one curve.

The interplay between gravity and inertia is further explored upon examining the flow at low Reynolds number. Figure 9 displays the influence of gravity on steady film and flow profiles for $Re = 20$, $Rv = 14$, $\varepsilon = 0.1$ and $De = 0.5$. In contrast to high-inertia flow (see figure 7), the flow experiences strong gradient in velocity and stress, particularly near the annulus exit, as a result of elastic effect. In this case, both velocity and stress exhibit strong over- and under-shoots coinciding with the sudden change in slope of the film surface. Figure 10 shows the evolution of the film for the low-inertia fluid under moderate gravitational effect ($1/Fr = 0.3$). In contrast to the flow in the absence of gravity (compare with figures 4 and 5), the flow does not evolve monotonically towards the steady state. In the beginning, the film surface experiences a relatively strong elevation near the annulus exit, with the film thickness decaying downstream close to its initial level. This original overshoot continues to strengthen with time until the film height reaches near steady-state level near $x = 0$, at which stage the film surface becomes wavy everywhere. The waviness, however, subsides with time as the film shape approaches asymptotically the steady state.

Finally, the similarity discussed above between figures 2 and 6, and the independence of the critical elasticity number on Reynolds number in figure 8, can be explained by rescaling the governing equations. Only some of the variables need to be rescaled, namely

$$x \to \frac{x}{Re}, \quad t \to \frac{t}{Re}, \quad u_z \to Reu_z, \quad \tau_{ii} \to \frac{\tau_{ii}}{Re}, \tag{3.8a}$$

where $i = x, y, z$. The rest of the variables remain unchanged. In this case, the continuity equation retains its original form, so that the conservation equations, (2.7*a*, *b*), now read,

$$u_{x,x} + \varepsilon u_z + u_{z,z} = 0, \tag{3.8b}$$

$$u_{x,t} + u_x u_{x,x} + u_z u_{x,z} = \frac{Re}{Fr^2} + aRv\,(u_{x,zz} + \varepsilon u_{x,z}) + \tau_{xx,x} + \tau_{zx,z} + \varepsilon\tau_{zx}, \tag{3.8c}$$

while the constitutive equations, (2.7*d*–*g*), become

$$E(\tau_{zz,t} + u_x\,\tau_{zz,x} + u_z\,\tau_{zz,z} - 2\tau_{zz}u_{z,z} - 2\tau_{zx}u_{z,x}) + \tau_{zz} = 2au_{z,z}, \tag{3.8d}$$

$$E(\tau_{yy,t} + u_x\,\tau_{yy,x} + u_z\,\tau_{yy,z} - 2\tau_{yy}u_z) + \tau_{yy} = \varepsilon au_z, \tag{3.8e}$$

$$E(\tau_{xx,t} + u_x\,\tau_{xx,x} + u_z\,\tau_{xx,z} - 2\tau_{zx}u_{x,z} - 2\tau_{xx}u_{x,x}) + \tau_{xx} = 0, \tag{3.8f}$$

$$E(\tau_{zx,t} + u_x\,\tau_{zx,x} + u_z\,\tau_{zx,z} - \tau_{zz}u_{x,z} + \varepsilon\tau_{zx}u_z - \tau_{xx}u_{z,x}) + \tau_{zx} = au_{x,z}. \tag{3.8g}$$

Clearly, there are now only two similarity parameters in the problem, namely Re/Fr^2 and E.

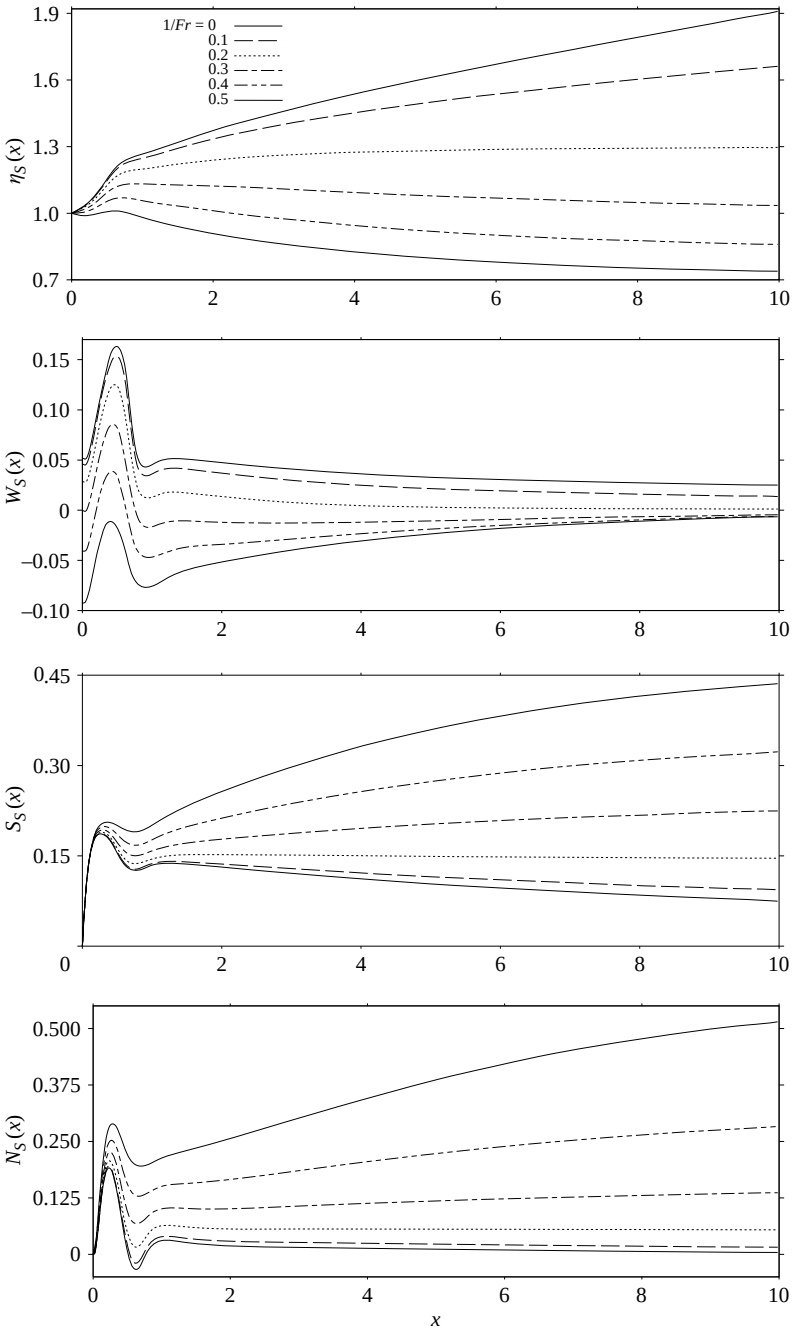

FIGURE 9. Influence of gravity on steady-state film height, mean radial velocity component, shear stress and normal stress, for a viscoelastic fluid with low inertia. $Re = 20$, $Rv = 1$, $\varepsilon = 0.1$, $De = 0.5$ and $1/Fr \in [0, 0.5]$.

3.3. *Influence of substrate topography*

In this section, the influence of substrate dimension and topography is examined. First, consider the influence of aspect ratio on a straight cylinder. Figure 11 displays steady-state film, velocity and stress profiles for $\varepsilon \in [0.1, 0.5]$, $Re = 100$, $De = 2.9$ and $Rv = 1$. The viscoelastic character of the flow is most evident when the flow is two-dimensional

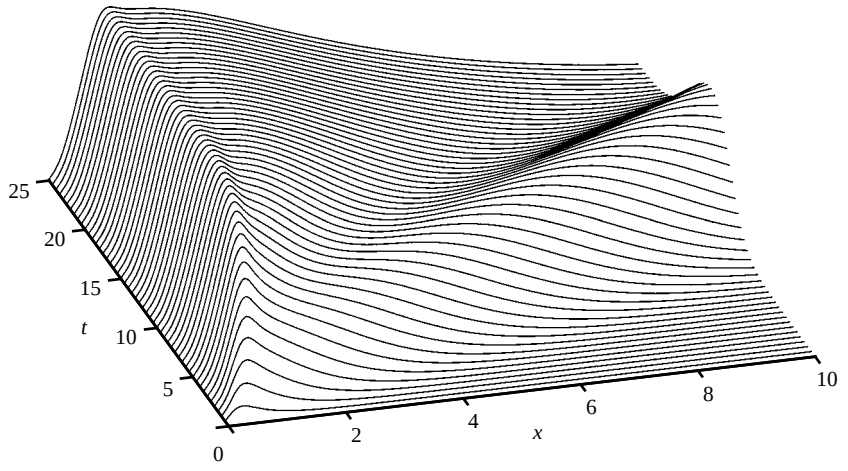

FIGURE 10. Transient flow response for low-inertia viscoelastic film, in the presence of gravity. $Re = 20$, $Rv = 1$, $\varepsilon = 0.1$, $De = 0.5$ and $1/Fr = 0.3$. The figure shows the evolution of the film height.

($\varepsilon = 0$). Thus, the effect of normal-stress is most palpable for a narrow gap or large inner cylinder radius, manifesting itself in the form of a wavy response. As ε increases (from zero), the waviness tends to subside. This is particularly evident from the mean radial velocity component. Generally, the flow strength decreases linearly with ε. Overall, however, there is little effect of ε on the film thickness and stress near the annulus exit.

So far, all results reported relate to a flow over a straight cylindrical substrate. In order to accentuate the effect of substrate topography on film flow, step changes in the cylindrical substrate are considered. This may at first seem to violate the thin-film hypothesis, according to which the film free surface must be smooth, with small slope, of $O(\varepsilon^2)$. This subsequently places a restriction on the substrate topography, which must also be smooth since both flow-field and free-surface shape depend directly on bottom topography. However, rapid or even discontinuous variation in substrate topography can, under certain conditions, have little impact on free-surface smoothness. Homsy and co-workers examined the flow over mounds and trenches for Stokes flow and strong surface-tension, using lubrication theory for thin-film flow (Kalliadasis *et al.* 2000), and a boundary-integral method for the fully two-dimensional problem (Mazouchi & Homsy 2001). Comparison between the two approaches led to excellent agreement despite the steep (discontinuous) variation in substrate topography. This agreement was attributed to strong surface-tension effects, which tend to smooth out the film free surface, thus ensuring the validity of the thin-film hypothesis. Whether fluid elasticity plays a smoothing role, similar to that of surface-tension, is an interesting and important question, which will shortly be examined through the current formulation. The influence of inertia and shear thinning/thickening have previously been examined by Khayat and co-workers. His variation in film surface appears to preserve the same steepness in shape as the substrate topography for a flow with inertia level (Khayat & Welke 2001), and any level of shear thinning/thickening (Kim & Khayat 2002).

A suitable substrate profile, corresponding to a step-up and/or a step-down, is taken from (Kalliadasis *et al.* 2000), which is written here in dimensionless form as

$$h(x) = \frac{A}{\pi}\left[\tan^{-1}\left(\frac{x - x_1}{\delta}\right) - \tan^{-1}\left(\frac{x - x_2}{\delta}\right)\right], \tag{3.9}$$

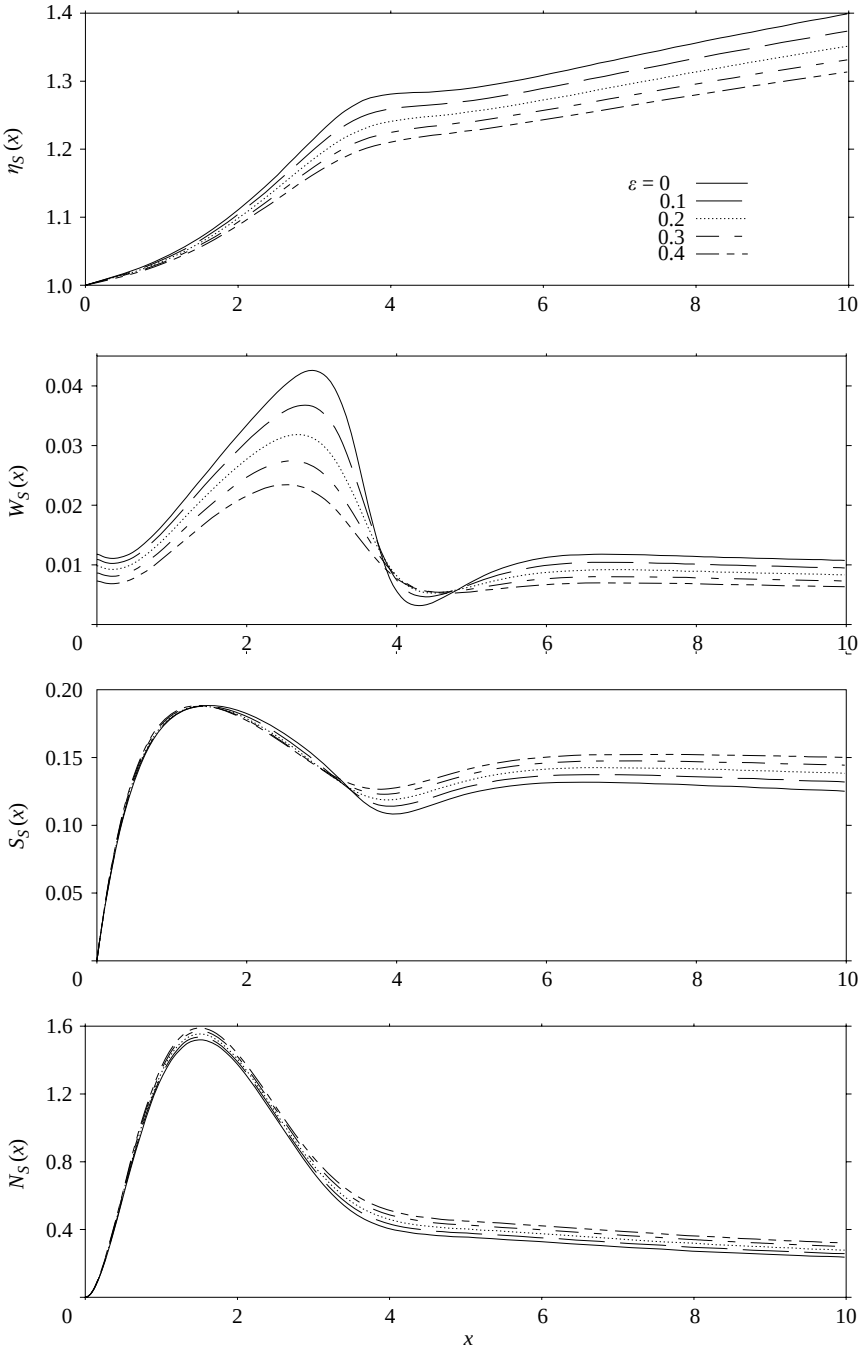

FIGURE 11. Influence of aspect ratio on steady-state film height, mean radial velocity, shear stress and normal stress, in the absence of gravity ($1/Fr = 0$). $Re = 100$, $Rv = 1$, $De = 2.9$ and $\varepsilon \in [0, 0.5]$.

where A is the amplitude of the step, δ is the slope, x_1 and x_2 are the locations of the step-up and step-down, respectively. In this work, $\delta = 0.1$. It is found that both the step-up and step-down disturbances have a significant and different influence on the flow.

Consider first the flow over a substrate with step-up topography ($x_2 \to \infty$). In this case, the influence of elasticity is illustrated in figure 12 for steady film flow on a substrate with $A = 0.5$ and $x_1 = 4$ ($Re = 100$, $Rv = 1$ and $\varepsilon = 0.1$). The influence of elasticity on the film height and shape should be compared to that of surface-tension from figure 7 in (Mazouchi & Homsy 2001). Several observations can be made. In contrast to the flow with dominant surface-tension effects, the presence of the step up does not seem to affect the flow upstream. This observation is confirmed upon comparing figures 2 and 12, particularly upon examining the level of normal stress. In addition, elasticity has little effect on the film shape and flow until it traverses the step. Both elasticity and surface-tension effects have a smoothing influence on the film height (and flow field). We may then speculate that the presence of steep variation in substrate topography tends to be smoothed out by elastic and surface-tension effects. The influence of elasticity is essentially felt in the shear and normal stresses. When the step is reached ($x = 4$), the flow experiences a localized and sharp increase in velocity and stress magnitude, which immediately subsides downstream of the step. This impulsive behaviour is expected since both $\eta_S(x)$ and $U_S(x)$ behave like $h(x)$, and consequently $W_S(x)$, $S_S(x)$ and $N_S(x)$ behave like $\mathrm{d}h/\mathrm{d}x$. The step causes the film height to increase slightly with elasticity, with essentially no change in radial flow. In contrast, both shear and normal stresses increase significantly with elasticity. The development of sharp stress gradients is likely to cause the film to rupture in this case. Recall from figures 2 and 5 that it is the sharpening of velocity and not stress gradient that is the primary mechanism for film rupture. In this regard, figure 13 shows the dependence of the critical Deborah number for film rupture on substrate amplitude and slope. Overall, a film will more probably rupture if the step slope is steeper. For a given slope, δ, the critical Deborah number increases linearly with A at small amplitude. At some value of A, De decreases rapidly with A, at a rate that is essentially independent of δ.

The evolution of the film for transient flow is shown in figure 14 for $De = 1$. There are roughly three flow regions at a given time. In the first region upstream of the step, $\eta(x, t)$ increases linearly with both x and t. This response is in sharp contrast with that experienced for a straight cylinder, where the film undergoes a non-monotonic elevation near the annulus exit (see figures 4 and 5). In the second region around or right downstream of the step, the film height exhibits a maximum, which quickly weakens with time, but remains localized. In the third region, far downstream, the film tends to thicken relatively quickly towards the steady state. In this regard, observe that the presence of the step tends to stabilize the flow as the steady state is reached earlier than for Newtonian film (figure 4), for a highly elastic film (figure 5), and for a film with low inertia in the presence of gravity (figure 10).

Finally, consider the flow over a rectangular step (up/down). In this case, $A = 0.5$, $x_1 = 4$ and $x_2 = 6$, with $Re = 100$, $Rv = 1$ and $\varepsilon = 0.1$. The steady-state profiles for film height, radial velocity and stress are shown in figure 15. The presence of the step-up and step-down leads to the opposite effect on the flow, which is reflected by the presence of maxima and minima; but perhaps the most striking feature in the figure is the presence of (kinematic) symmetry in film height and antisymmetry in velocity between the upward and the downward flow regions, and the absence of (dynamic) symmetry in stress. This is particularly evident from the velocity and stress profiles, where $W_S(x = 4) = -W_S(x = 6)$, and $S_S(x = 4) \gg S_S(x = 6)$. The presence of strong stress gradient in the upward region suggests that the film is likely to rupture before it traverses the entire bump. Consequently, the values of the critical Deborah number for film rupture reported in figure 13 are the same for the flow over a square bump.

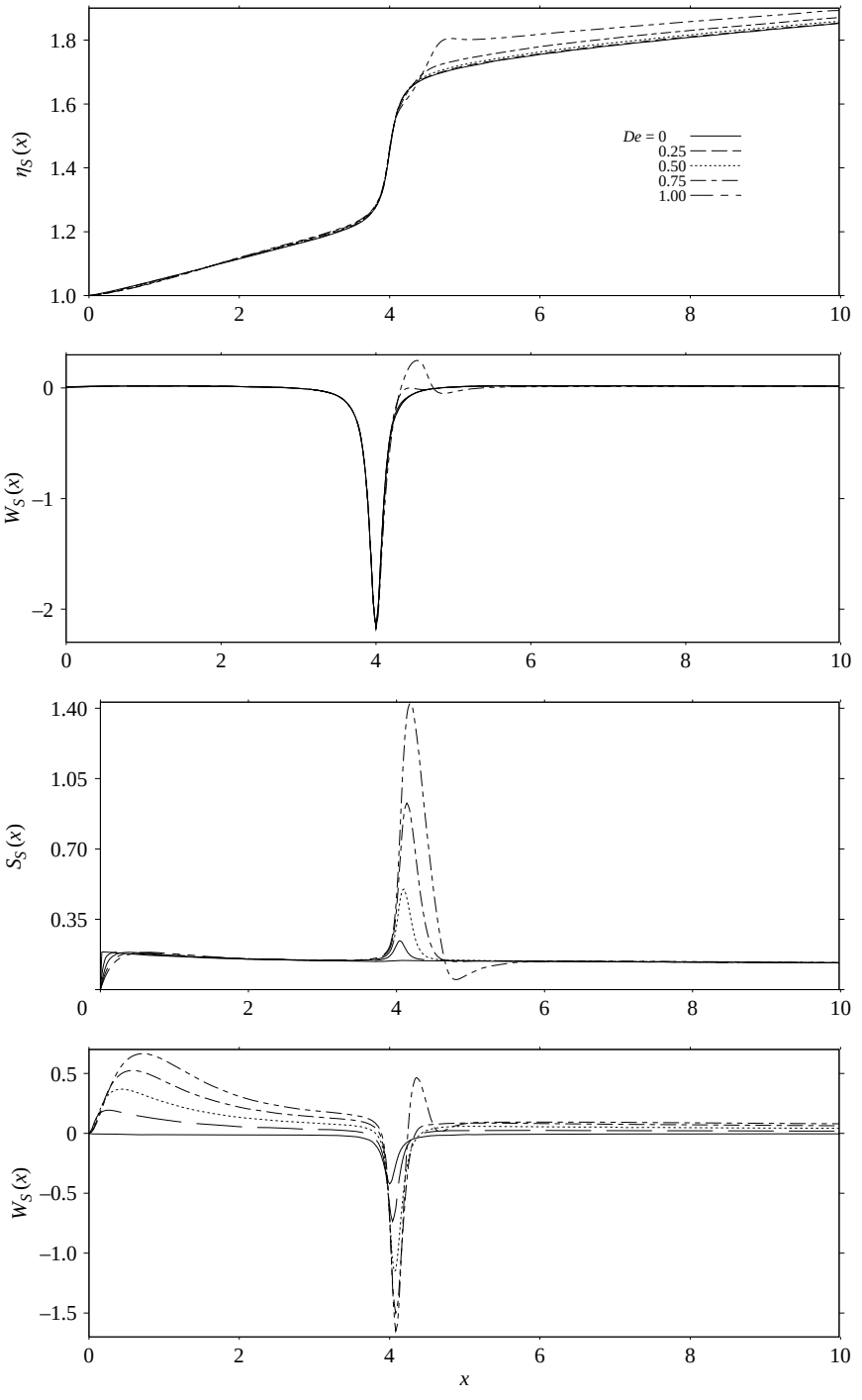

FIGURE 12. Influence of elasticity on steady-state film height, mean radial velocity, shear stress and normal stress, in the absence of gravity ($1/Fr = 0$), for a flow over a cylindrical substrate with a step-up topography ($A = 0.5$, $\delta = 0.1$, $x_1 = 4$ and $x_2 \to \infty$). $Re = 100$, $Rv = 1$, $\varepsilon = 0.1$ and $De \in [0, 1]$.

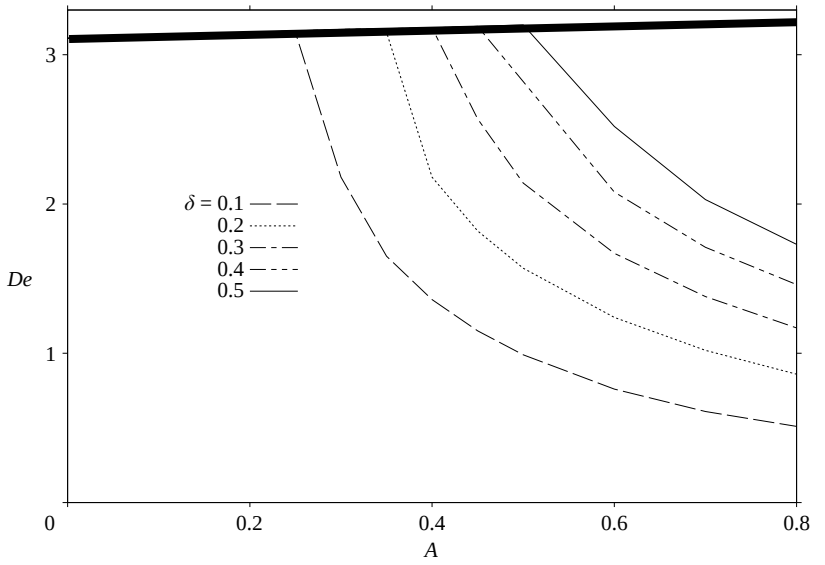

FIGURE 13. Dependence of the critical Deborah number for film rupture on step-up substrate amplitude for various slopes, in the absence of gravity ($1/Fr = 0$). $Re = 100$ and $\varepsilon = 0.1$.

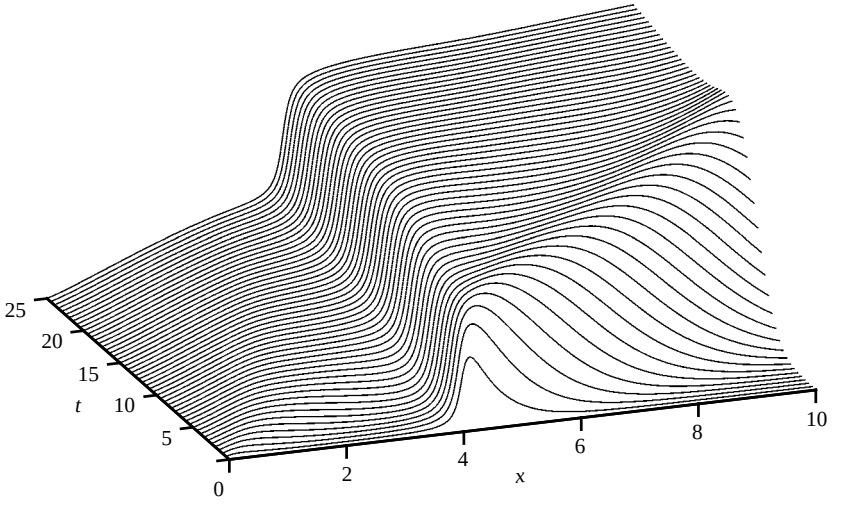

FIGURE 14. Transient film flow over a cylindrical substrate with a step-up topography ($A = 0.5$, $\delta = 0.1$, $x_1 = 4$ and $x_2 \to \infty$). $Re = 100$, $Rv = 1$, $\varepsilon = 0.1$ and $De = 1$.

4. Concluding remarks

The axisymmetric viscoelastic flow of a thin fluid film, emerging from an annulus, is examined in this study. The problem is of direct relevance to the early stages of fibre or wire coating. The Oldroyd-B type constitutive model is adopted. The effect of substrate topography as well as the influence of fluid elasticity, inertia and gravity is investigated. The thin-film equations are solved by expanding the flow field and stress in terms of orthonormal modes in the radial direction, and using Galerkin projection. The one-mode expansion is equivalent to the depth-averaging formulation. Steady and transient flows are examined.

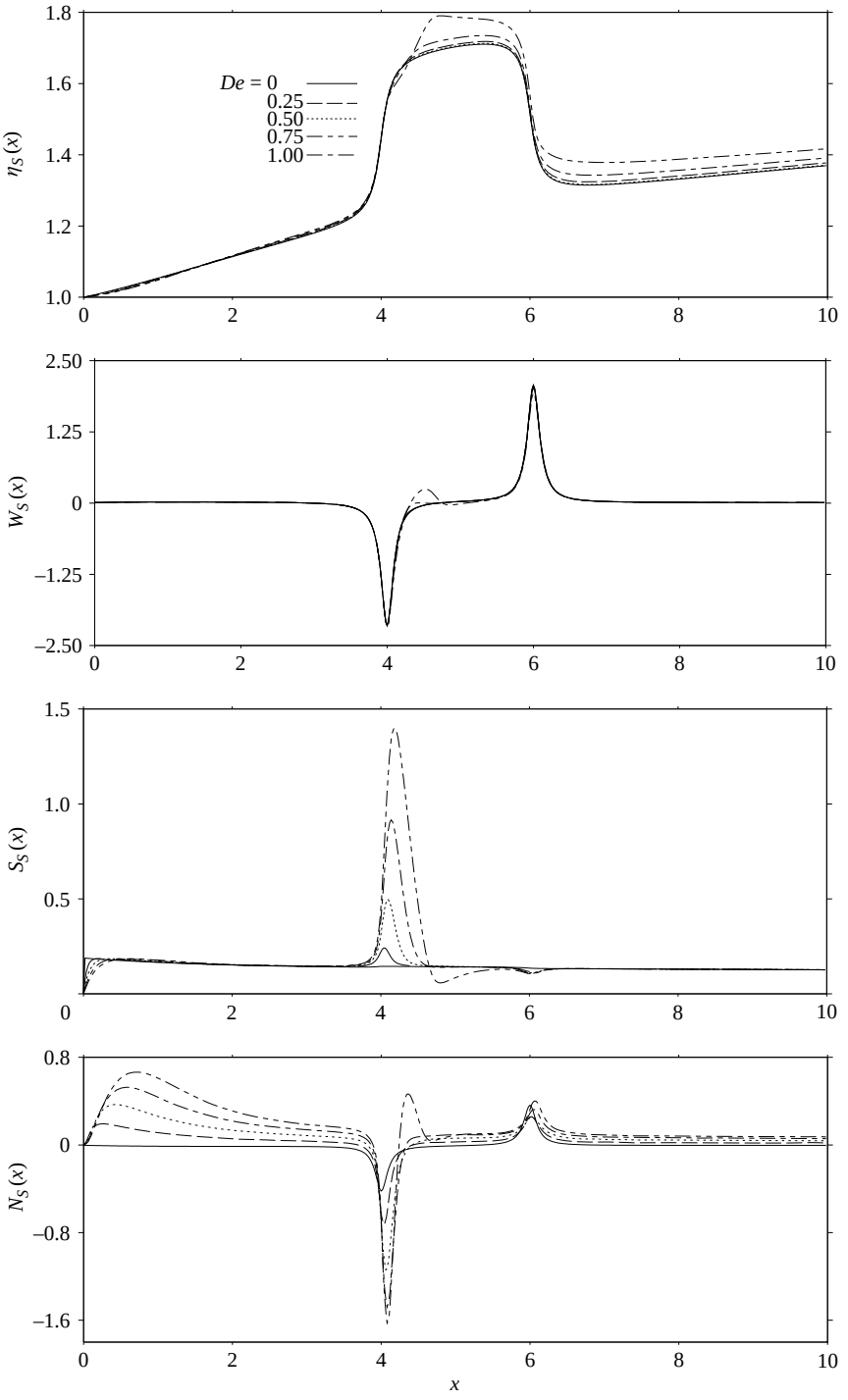

FIGURE 15. Influence of elasticity on steady-state film height, mean radial velocity, shear stress and normal stress, in the absence of gravity ($1/Fr = 0$), for a flow over a cylindrical substrate with a step-up/down topography ($A = 0.5$, $\delta = 0.1$, $x_1 = 4$ and $x_2 = 6$). $Re = 100$, $Rv = 1$, $\varepsilon = 0.1$ and $De \in [0, 1]$.

It is found that Newtonian and weakly elastic steady films exhibit some swelling near the annulus exit and a monotonically increasing film thickness. In contrast, moderately to strongly elastic films develop waviness, which is accompanied by strong velocity gradient and stress. The gradient steepens with elasticity, towards a shock, which is accompanied by strong normal stress buildup, thus leading to film rupture. Shock formation is also predicted for elastic transient flow. In contrast to Newtonian films, elastic films tend to rupture and do not reach steady state. It is also found that a film with both low inertia and elasticity behaves very differently from a film with both high inertia and elasticity. A sudden change in surface slope is predicted in the former case, which is reminiscent of phase transition. Gravity is found to have a non-monotonic influence on the onset of waviness and rupture. Low and high gravitational forces tend to be stabilizing for the film (figure 8). As to the influence of substrate topography, it is found that a film flowing on a straight smaller gap-to-radius ratio cylinder tends to be less stable. The presence of a step-up and/or step-down on the substrate can lead to substantial stress buildup, but the effect is not symmetric; there is relatively negligible stress buildup for a film in the step-down region in comparison to the step-up region, despite the symmetry in flow kinematics (figure 15). Similarly to surface-tension, elasticity tends to have a smoothing influence on the film free surface. Consequently, for a viscoelastic fluid with negligible surface-tension, the thin-film hypothesis is expected to hold in the presence of steep variation in substrate topography. This is not the case for Newtonian (Khayat & Welke 2001) and generalized Newtonian (Kim & Khayat 2002) fluids.

A number of assumptions were made in the current study, which must be relaxed for more realistic predictions to be reached. For instance, practical polymeric fluids tend to display shear thinning of strain hardening, along with a spectrum of relaxation times, which have not been accounted for here. Although film breakup or rupture is not the major focus in this study, surface-tension, which has been neglected here, is expected to play an important role at least in the final breakup phase, even for polymeric fluids. At the breakup stage, the local curvature of the film surface becomes significant enough for surface-tension to cease to be negligible. Simultaneously, the thin-film assumption ceases to be valid altogether. For further discussion on nonlinear breakup in polymeric free-surface flows, see the review by Eggers (1997).

This work is supported by the Natural Sciences and Engineering Research Council of Canada.

Appendix A. Scaled equations

Upon introducing the dimensionless variables from (2.6) into equations (2.1)–(2.3), the relevant equations for the problem reduce to

$$u_{x,x} + \varepsilon u_z + u_{z,z} = 0, \tag{A 1}$$

$$Re(u_{x,t} + u_x u_{x,x} + u_z u_{x,z}) = -p_{,x} + \frac{Re}{Fr^2} + aRv(u_{x,zz} + \varepsilon u_{x,z}) + \tau_{xx,x} + \varepsilon^{2-\alpha}\tau_{zx,z} + \varepsilon\tau_{zx}, \tag{A 2}$$

$$p_{,z} = \varepsilon^{2-\gamma}\,\tau_{zz,z} + \varepsilon^2\,\tau_{zx,x} + \varepsilon^{2-\gamma}\,\tau_{zz} + \varepsilon^{2-\beta}\,\tau_{yy}, \tag{A 3}$$

$$De[\varepsilon^{-\gamma}\,(\tau_{zz,t} + u_z\tau_{zz,z} + u_x\tau_{zz,x} - 2\tau_{zz}u_{z,z}) - 2\tau_{zx}u_{z,x}] + \varepsilon^{-\gamma}\tau_{zz} = 2\,a\,u_{z,z}, \tag{A 4}$$

$$De\varepsilon^{-\beta}[\tau_{yy,t} + u_x\tau_{yy,x} + u_z\tau_{yy,z} - 2\,\tau_{yy}u_z] + \varepsilon^{-\beta}\tau_{yy} = \varepsilon a u_z, \tag{A 5}$$

$$De[\varepsilon^{-\alpha}(\tau_{xx,t} + u_x\tau_{xx,x} + u_z\tau_{xx,z} - 2\tau_{zx}u_{x,z}) - 2\varepsilon^{-2}\tau_{xx}u_{x,x}] + \varepsilon^{-\alpha}\tau_{xx} = a u_{x,x}, \tag{A 6}$$

$$De[\tau_{zx,t} + u_x\tau_{zx,x} + u_z\tau_{zx,z} - \varepsilon^{-\gamma}\tau_{zz}u_{x,z} - \tau_{zx}u_{x,x} - \tau_{zx}u_{z,z} - \varepsilon^{2-\alpha}\tau_{xx}u_{z,x}] + \tau_{zx} = a\,u_{x,z}. \tag{A 7}$$

Appendix B. Shape functions

In this Appendix, the shape functions are given explicitly for the first three modes. Thus, the shape functions, $\phi_i(\xi)$, for velocity are given by

$$\phi_1(\xi) = \frac{\sqrt{30}}{16}(-4\xi^2 + 4\xi + 3), \quad \phi_2(\xi) = \frac{\sqrt{546}}{208}(128\xi^3 - 52\xi^2 - 44\xi + 7),$$
$$\phi_3(\xi) = \frac{3\sqrt{286}}{4576}(7280\xi^4 - 2016\xi^3 - 2496\xi^2 + 368\xi + 101).$$

The shape functions, $\psi_i(\xi)$, for the shear stress are:

$$\psi_1(\xi) = \sqrt{30}\big(-\xi + \tfrac{1}{2}\big), \quad \psi_2(\xi) = \frac{\sqrt{5}}{2}(-8\xi^2 + 2\xi + 1),$$
$$\psi_3(\xi) = \frac{\sqrt{7}}{8}(120\xi^3 - 20\xi^2 - 22\xi + 1).$$

Finally, the shape functions, $\theta_i(\xi)$, for normal stress are:

$$\theta_1(\xi) = \frac{\sqrt{30}}{16}(-4\xi^2 - 4\xi + 3), \quad \theta_2(\xi) = \frac{\sqrt{546}}{208}(-128\xi^3 - 52\xi^2 + 44\xi + 7),$$
$$\theta_3(\xi) = \frac{3\sqrt{286}}{4576}(7280\xi^4 + 2016\xi^3 - 2496\xi^2 - 368\xi + 101).$$

Appendix C. Projected equations (N-modes)

The Galerkin projection is carried out by using expressions (2.12) and multiplying each of equations (2.7) by the appropriate weight function. Letting $A = -\Delta_{,x}/\Delta$, $B = -\Sigma_{,x}/2\Delta$ and $C = -\eta_{,t}/\Delta$, the x-momentum conservation equation (2.7b) reads:

$$\begin{aligned}
&Re[U_{i,t} + C\langle(\xi + 1/2)\phi_i\phi_j'\rangle U_j + (\langle\phi_i\phi_j\phi_k\rangle + \varepsilon\Delta\langle\phi_i\phi_j'(F_k\xi - G_k)\rangle - \langle\phi_i\phi_j'F_k\rangle)U_jU_{k,x}\\
&+\{A(\langle\phi_i\phi_j'(F_k - \phi_k\xi)\rangle + \langle\phi_i\phi_j\phi_k'\xi\rangle) + \varepsilon\Delta B\langle\phi_i\phi_j'F_k\rangle - \varepsilon\Delta A\langle\phi_i\phi_j'(F_k\xi - 2G_k)\rangle\}U_jU_k]\\
&= \frac{Re}{Fr^2}\langle\phi_i\rangle + a\,Rv\left(\frac{1}{\Delta^2}\langle\phi_i\phi_j''\rangle + \frac{\varepsilon}{\Delta}\langle\phi_i\phi_j'\rangle\right)U_j + \langle\phi_i\theta_j\rangle Q_{j,x} + (A\langle\phi_i\theta_j'\xi\rangle + B\langle\phi_i\theta_j'\rangle)Q_j\\
&\quad + \left(\frac{1}{\Delta}\langle\phi_i\psi_j'\rangle + \varepsilon\langle\phi_i\psi_j\rangle\right)S_j
\end{aligned}$$

whereas the stress equation (7b) for τ_{xx} is given by

$$\begin{aligned}
De\Big[&Q_{i,t} + C\langle(\xi + \tfrac{1}{2})\theta_i\theta_j'\rangle Q_j + \langle\theta_i\phi_j\theta_k\rangle U_jQ_{k,x} + (\varepsilon\Delta\langle\theta_i\theta_j'(F_k\xi - G_k)\rangle - \langle\theta_i\theta_j'F_k\rangle\\
&-2\langle\theta_i\theta_j\phi_k\rangle)Q_jU_{k,x} + \{A\langle\theta_i\phi_j\theta_k'\xi\rangle + B\langle\theta_i\phi_j\theta_k'\rangle\}U_jQ_k + \{A(\langle\theta_i\theta_j'(F_k - \phi_k\xi)\rangle\\
&-2\langle\theta_i\theta_j\phi_k'\xi\rangle) - B(2\langle\theta_i\theta_j\phi_k'\rangle + \langle\theta_i\theta_j'\phi_k\rangle) - \varepsilon\Delta A\langle\theta_i\theta_j'(F_k\xi - 2G_k)\rangle\\
&+\varepsilon\Delta B\langle\theta_i\theta_j'F_k\rangle\}Q_jU_k - \frac{2}{\Delta}\langle\theta_i\phi_j'\psi_k\rangle U_jS_k\Big] + Q_i = 0
\end{aligned}$$

that for τ_{zz},

$$\begin{aligned}
De\big[&R_{i,t} + C\big\langle\big(\xi + \tfrac{1}{2}\big)\theta_i\theta_j'\big\rangle R_j + \langle\theta_i\phi_j\theta_k\rangle U_jR_{k,x} + \{\varepsilon\Delta(\langle\theta_i\theta_j'(F_k\xi - G_k)\rangle - 2\langle\theta_i\theta_jF_k\rangle)\\
&+2\langle\theta_i\theta_j\phi_k\rangle - \langle\theta_i\theta_j'F_k\rangle\}R_jU_{k,x} + \{\varepsilon\Delta A(2\langle\theta_i\theta_j(F_k - \phi_k\xi)\rangle - \langle\theta_i\theta_j'(F_k\xi - 2G_k)\rangle)\\
&+\varepsilon\Delta B(\langle\theta_i\theta_j'F_k\rangle - 2\langle\theta_i\theta_j\phi_k\rangle) + A(\langle\theta_i\theta_j'(F_k - \phi_k\xi)\rangle + 2\langle\theta_i\theta_j\phi_k'\xi\rangle) - B(\langle\theta_i\theta_j'\phi_k\rangle\\
&-2\langle\theta_i\theta_j\phi_k'\rangle)\}R_jU_k - 2\langle\theta_i\psi_ju_{z,x}\rangle S_j\big] + R_i = 2a\{\varepsilon\Delta\langle\theta_iF_j\rangle - \langle\theta_i\phi_j\rangle\}U_{j,x}\\
&-2a\{A\langle\theta_i\phi_j'\xi\rangle + B\langle\theta_i\phi_j'\rangle + \varepsilon\Delta A\langle\theta_i(F_j - \phi_j\xi)\rangle - \varepsilon\Delta B\langle\theta_i\phi_j\rangle\}U_j\}
\end{aligned}$$

and the equation for τ_{zx} is

$$
\begin{aligned}
De\big[S_{i,t} + C\big\langle\big(\xi+\tfrac{1}{2}\big)\psi_i\psi_j'\big\rangle S_j + \langle\psi_i\phi_j\psi_k\rangle U_j S_{k,x} + \{\varepsilon\Delta(\langle\psi_i\psi_j'(F_k\xi - G_k)\rangle - \langle\psi_i\psi_j F_k\rangle)\\
- \langle\psi_i\psi_j' F_k\rangle + \langle\psi_i\psi_j\phi_k\rangle\}S_j U_{k,x} + \{A\langle\psi_i\psi_j'(F_k-\phi_k\xi)\rangle - B\langle\psi_i\psi_j'\phi_k\rangle\\
+ \varepsilon\Delta A(\langle\psi_i\psi_j(F_k-\phi_k\xi)\rangle - \langle\psi_i\psi_j'(F_k\xi-2G_k)\rangle) + \varepsilon\Delta B(\langle\psi_i\psi_j' F_k\rangle - \langle\psi_i\psi_j\phi_k\rangle)\}S_j U_k\\
- \frac{1}{\Delta}\langle\psi_i\phi_j'\theta_k\rangle U_j R_k + \{A\langle\psi_i\phi_j\psi_k'\xi\rangle + B\langle\psi_i\phi_j\psi_k'\rangle\}U_j S_k - \langle\psi_i\theta_j u_{z,x}\rangle Q_j\big] + S_i\\
= \frac{a}{\Delta}\langle\psi_i\phi_j'\rangle U_j.
\end{aligned}
$$

Note that

$$
\begin{aligned}
u_{z,x} = {} & \Delta[-F_k + \varepsilon\Delta(F_k\xi - G_k)]U_{k,xx}\\
& + \Delta[2A(F_k-\phi_k\xi) - 2B\phi_k - 2\varepsilon\Delta A(F_k\xi - 2G_k) + 2\varepsilon\Delta B F_k]U_{k,x}\\
& + \Delta[(A_{,x} - A^2)(F_k - \phi_k\xi) + (AB - B_{,x})\phi_k - A^2\phi_k'\xi - B^2\phi_k' - AB\phi_k'(\xi+1)\\
& - \varepsilon\Delta\big(A_{,x} - 2A^2\big)(F_k\xi - 2G_k) + \varepsilon\Delta(B_{,x} - AB)F_k + +\varepsilon\Delta B^2\phi_k\\
& - \varepsilon\Delta A^2(F_k - \phi_k\xi)\xi]U_k.
\end{aligned}
$$

Finally, the kinematic condition (2.9) leads to the following equation for $\eta(x,t)$:

$$
\begin{aligned}
\eta_{,t}(x,t) = {} & \Delta\sum_{k=1}^{M}\left[\varepsilon\Delta\left(\frac{F_k^+}{2} - G_k^+\right) - F_k^+\right]U_{k,x}\\
& - \sum_{k=1}^{M}\left[\Delta_{,x}\left(F_k^+ - \frac{\phi_k^+}{2}\right) - \frac{\sum_{,x}}{2}\phi_k^+ - \varepsilon\Delta\Delta_{,x}\left(\frac{F_k^+}{2} - 2G_k^+\right) + \varepsilon\Delta\frac{\sum_{,x}}{2}F_k^+ - \phi_k^+\eta_{,x}\right]U_k,
\end{aligned}
$$

Appendix D. Constants for the depth-averaged equations

The constants in equations (3.1) are introduced in this appendix. Subscript 1 is dropped from the shape functions.

$$
C_1 = \frac{\langle\phi\rangle^3}{\langle\phi^3\rangle} = 0.648, \quad C_2 = \frac{\langle\phi\phi''\rangle}{\langle\phi^3\rangle\langle\phi\rangle} = -2.333, \quad C_3 = \frac{\langle\phi\rangle^2\langle\phi\theta\rangle}{\langle\phi^3\rangle\langle\theta\rangle} = 0.535,
$$

$$
C_4 = \frac{\langle\phi\rangle^2\big\langle\phi\theta'\big(\xi+\frac{1}{2}\big)\big\rangle}{\langle\phi^3\rangle} = -0.789, \quad C_5 = \frac{\langle\phi\rangle\langle\phi\psi'\rangle}{\langle\phi^3\rangle\langle\psi\rangle} = -1.42,
$$

$$
C_6 = 2\frac{\big\langle\theta^2\big[\phi + \phi'\big(\xi+\frac{1}{2}\big)\big]\big\rangle}{\langle\theta^2\phi\rangle} = 3.407, \quad C_7 = 2\frac{\langle\phi\rangle\langle\theta\rangle\big\langle\theta\psi\phi'\big(\xi+\frac{1}{2}\big)\big\rangle}{\langle\psi\rangle\langle\theta^2\phi\rangle} = 1.262,
$$

$$
C_8 = 2\frac{\langle\phi\rangle\langle\theta\rangle\big\langle\theta\psi\phi\big(\xi+\frac{1}{2}\big)\big\rangle}{\langle\psi\rangle\langle\theta^2\phi\rangle} = 0.699, \quad C_9 = -2\frac{\langle\theta\rangle\big\langle\theta\big[\phi + \phi'\big(\xi+\frac{1}{2}\big)\big]\big\rangle}{\langle\theta^2\phi\rangle} = -3.111,
$$

$$
C_{10} = -2\frac{\big\langle\theta^2\big[\phi + \phi'\big(\xi+\frac{1}{2}\big)\big]\big\rangle}{\langle\theta^2\phi\rangle} = -3.407, \quad C_{11} = -2\frac{\langle\theta\rangle\langle\theta\phi'\psi\rangle}{\langle\phi\rangle\langle\psi\rangle\langle\theta^2\phi\rangle} = -4.454,
$$

$$
C_{12} = \frac{\langle\psi\rangle\langle\phi\rangle\big\langle\theta\psi\phi'\big(\xi+\frac{1}{2}\big)\big\rangle}{\langle\theta\rangle\langle\psi^2\phi\rangle} = 0.685, \quad C_{13} = \frac{\langle\psi\rangle\langle\phi\rangle\big\langle\theta\psi\phi\big(\xi+\frac{1}{2}\big)\big\rangle}{\langle\theta\rangle\langle\psi^2\phi\rangle} = 0.379,
$$

$$
C_{14} = -\frac{\langle\psi\rangle\langle\psi\phi'\theta\rangle}{\langle\phi\rangle\langle\theta\rangle\langle\psi^2\phi\rangle} = 3.081, \quad C_{15} = \frac{\langle\psi\rangle\langle\psi\phi'\rangle}{\langle\phi\rangle\langle\psi^2\phi\rangle} = 4.108,
$$

$$
C_{16} = -\big\langle\psi\big(\xi+\tfrac{1}{2}\big)\big\rangle = -0.571, \quad \alpha = \frac{\langle\phi\rangle}{\langle\theta^2\phi\rangle} = 1.667, \quad \beta = \frac{\langle\phi\rangle}{\langle\psi^2\phi\rangle} = 1.383.
$$

REFERENCES

Alekseenko, S. V., Nakoryakov, V. E. & Pokusaev, B. G. 1985 Wave formation on a vertical falling liquid film. *AIChE J.* **31**, 1446.

Balmforth, N. J. & Mandre, S. 2004 Dynamics of roll waves. *J. Fluid Mech.* **514**, 1.

Behrens, R. A., Crochet, M. J. Denson, C. D. & Metzner, A. B. 1987 Transient free-surface flows: motion of a fluid advancing in a tube. *AIChE J.* **33**, 1178.

Benney, D. J. 1966 Long waves in liquid films. *J. Math. Phys.* **45**, 150.

Bertschy, J. R., Chin, R. W. & Abernathy, F. H. 1993 High-strain-rate free-surface boundary-layer flows. *J. Fluid Mech.* **216**, 443.

Bhatara, A., Shaqfeh, E. S. & Khomani, B. 2004 Influence of viscoelasticity on the interfacial dynamics of air displacing fluid flows – a computational study. *J. Non-Newtonian Fluid Mech.* **122**, 313.

Bird, R. B., Armstrong, R. C. & Hassager, O. 1987. *Dynamics of Polymeric Liquids*, vol. 1, 2nd edn. John Wiley.

Brourgin, P. 1997 Fluid mechanics of coating processes. *Proc. 2nd European Coating Symp. (Euromech 367), Strasbourg, France*, pp. 22–25.

de Bruyn, J. R. 1997 Crossover between surface-tension and gravity-driven instabilities of a thin fluid layer on a horizontal cylinder. *Phys. Fluids* **9**, 1599.

Burelbach, J. P., Bankoff, S. G. & Davis, S. H. 1988 Nonlinear stability of evaporating/condensing liquid films. *J. Fluid Mech.* **195**, 463.

Chang, H. C. 1994 Wave evolution on a falling film. *Annu. Rev. Fluid Mech.* **26**, 103.

Christanti, Y. & Walker, L. M. 2001 Surface-tension driven jet break up of strain-hardening polymer solutions. *J. Non-Newtonian Fluid Mech.* **100**, 9.

Eggers, J. 1997 Nonlinear dynamics and breakup of free surface flows. *Rev. Mod. Phys.* **69**, 865.

Fomin, S., Hashida, T. & Watterson, J. 2003 Fundamentals of steady-state non-Newtonian rimming flow. *J. Non-Newtonian Fluid Mech.* **111**, 19.

Frenkel, A. L. 1992 Nonlinear theory of strongly undulating thin films flowing down vertical surfaces. *Europhys. Lett.* **18**, 583.

Gordon, M., Yerushalmi, J. & Shinnar, R. 1973 Instability of jets of non-Newtonian fluids. *Trans. Soc. Rheol.* **17**, 303.

Goren, S. L. & Wronski, S. 1966 The shape of low-speed capillary jets of Newtonian liquids. *J. Fluid Mech.* **25**, 185.

Huzyak, P. C. & Koelling, K. W. 1997 The penetration of a long bubble through a viscoelastic fluid in a tube. *J. Non-Newtonian Fluid Mech.* **71**, 73.

Kalliadasis, S., Bielarz, C. & Homsy, G. M. 2000 Steady free-surface thin film flows over topography. *Phys. Fluids* **12**, 1889.

Kalliadasis, S. & Chang, H. C. 1994 Drop formation during coating of vertical fibres. *J. Fluid Mech.* **261**, 135.

Kang, F. & Chen, K. P. 1995 Nonlinear elastic instability of gravity-driven flow of a thin viscoelastic film down an inclined plane. *J. Non-Newtonian Fluid Mech.* **57**, 243.

Khayat, R. E. & Kim, K. 2002 Influence of initial conditions on transient two-dimensional thin-film flow. *Phys. Fluids* **14**, 4448.

Khayat, R. E. & Pan, R. 2004 Transient free-surface flow of a viscoelastic fluid in a narrow channel. *Intl J. Numer. Meth. Fluids* **46**, 637–661.

Khayat, R. E. & Welke, S. 2001 Influence on inertia, gravity and substrate topography on the two-dimensional transient coating flow of a thin Newtonian fluid film. *Phys. Fluids* **13**, 355.

Kim, K. & Khayat, R. E. 2002 Transient coating flow of non-Newtonian fluid film. *Phys. Fluids* **14**, 2202.

Kistler, S. F. & Schweizer, P. M. 1997 *Liquid Film Coating*. Chapman & Hall.

Kriegsmann, J. J., Miksis, M. J. & Vanden-Broek, J. 1998 Pressure driven disturbances on a thin viscous film. *Phys. Fluids* **10**, 1249.

Kumar, K. A. & Graham, M. D. 2000. Buckling instabilities in models of viscoelastic flows. *J. Non-Newtonian Fluid Mech.* **89**, 337.

Larson, R. G. 1992 Instability of viscoelastic flows. *Rheol. Acta* **31**, 213.

Leal, L. G. 1992 *Laminar Flow and Convective Transport Processes*. Butterworth–Heinemann.

Lee, A., Shaqfeh, E. S. & Khomani, B. 2002 A study of viscoelastic free surface flows by the finite-element method: Hele-Shaw and slot coating flows. *J. Non-Newtonian Fluid Mech.* **108**, 327.

Lee, J. & Mei, C. C. 1996 Stationary waves on an inclined sheet of viscous fluid at high Reynolds and Weber number. *J. Fluid Mech.* **307**, 191.

Mashayek, F. & Ashgriz, N. 1995 Instability of liquid coatings on cylindrical surfaces. *Phys. Fluids* **7**, 2143.

Mazouchi, A. & Homsy, G. M. 2001 Free surface Stokes flow over topography. *Phys. Fluids* **13**, 2751.

Meyers, T. G. 1998 Thin films with high surface-tension. *SIAM Rev.* **40**, 441.

Middleman, S. 1977 *Fundamental of Polymer Processing*. McGraw-Hill.

Middleman, S. 1995 *Modeling Axisymmetric Flows*. Academic.

Nguyen, L. T. & Balakotaiah, V. 2000 Modeling and experimental studies of wave evolution on free falling viscous films. *Phys. Fluids* **9**, 2236.

Omodei, B. J. 1979 Computer solutions of a plane Newtonian jet with surface-tension. *Comput. Fluids* **7**, 79.

Oron, A., Davis, S. H. & Bankoff, S. G. 1997 Long-scale evolution of thin liquid film. *Rev. Mod. Phys.* **69**, 931.

Pasquali, M. & Scriven, L. E. 2002 Free surface flows of polymer solutions with models based on the conformation tensor. *J. Non-Newtonian Fluid Mech.* **108**, 363.

Prokopiou, T., Cheng, M. & Chang, H. C. 1991 Long waves on inclined films at high Reynolds number. *J. Fluid Mech.* **222**, 665.

Pumir, A., Manneville, P. & Pomeau, Y. 1983 On solitary waves running down an inclined plane. *J. Fluid Mech.* **135**, 27.

Quéré, D. 1999 Fluid coating on a fibre. *Annu. Rev. Fluid Mech.* **31**, 347.

Reichl, L. E. 1984 *A Modern Course in Statistical Physics*. University of Texas Press, Austin.

Ro, J. S. & Homsy, G. M. 1995 Viscoelastic free surface flows: thin film hydrodynamics of Hele-Shaw and dip coating flow. *J. Non-Newtonian Fluid Mech.* **57**, 203.

Ruschak, K. J. & Weinstein, S. J. 1999 Viscous thin-film flow over a rounded crested weir. *Trans. ASME* I: *J. Fluid Engng* **121**, 673.

Ruyer-Quil, C. & Manneville, P. 1998 Modeling film flows down inclined planes. *Eur. J. Phys.* B **6**, 277.

Salamon, T. R., Armstrong, R. C. & Brown, R. A. 1994 Traveling waves on vertical films: numerical analysis using the finite-element method. *Phys. Fluids* **6**, 2202.

Shkadov, V. Y. 1967 Wave conditions of a flow in a thin viscous layer under the action of gravitational forces. *Izv. Akad. Nauk. SSSR Mehk. Zhid. Gaza,* **1**, 43.

Spaid, M. A. & Homsy, G. M. 1994 Viscoelastic free surface flows: spin coating and dynamic contact lines. *J. Non-Newtonian Fluid Mech.* **55**, 249.

Stansby, P. K. & Feng, T. 2005 Kinematics and depth-integrated terms in surf zone waves from laboratory measurements. *J. Fluid Mech.* **529**, 279.

Szeri, A. Z. 1987 Some extensions of the lubrication theory of Osborne Reynolds. *Trans. ASME J. Tribol.* **109**, 21.

Takeshi, O. 1999 Surface equation of falling film flows with moderate Reynolds number and large but finite Weber number. *Phys. Fluids* **11**, 3247.

Tanner, R. I. 1999 *Engineering Rheology*. Oxford University Press.

Tuck, E. O. & Bentwich, M. 1983 Sliding sheets: lubrication with comparable viscous and inertia forces. *J. Fluid Mech.* **135**, 51.

Voit, S. S. 1987 Tsunamis. *Annu. Rev. Fluid Mech.* **19**, 217.

Watson, E. J. 1964 The radial spread of a liquid jet over a horizontal plane. *J. Fluid Mech.* **20**, 481.

Weinstein, S. J. & Ruschak, K. J. 2004 Coating flow. *Annu. Rev. Fluid Mech.* **36**, 29.

Wilkes, J. O. & Nedderman, R. M. 1962 The measurement of velocities in thin film of liquid. *Chem. Engng Sci.* **17**, 177.

Zhang, Y. L. Matar, O. K. & Craster, R. V. 2002 Surfactant spreading on a thin weakly viscoelastic film. *J. Non-Newtonian Fluid Mech.* **105**, 53.

Zienkievicz, O. C. & Heinrich, J. C. 1979 A unified treatment of steady-state shallow water and two-dimensional Navier–Stokes equations – finite-element penalty function approach. *Comput. Meth. Appl. Mech. Engng* **17/18**, 673.